TECHNISCHE
UNIVERSITÄT
WIEN

DIPLOMARBEIT

Deep Inelastic Scattering and the WSS Model: A Study of Holographic Pomeron Exchange

zur Erlangung des akademischen Grades
Diplom-Ingenieur

ausgeführt am
E136-Institut für Theoretische Physik
der Technischen Universität Wien

unter der Anleitung von
Univ.-Prof. DI Dr. Anton Rebhan

Unterschrift des Betreuers

eingereicht von
Christian Mayrhofer
Matrikelnummer 01527418

Unterschrift des Studenten

October 15, 2024

Abstract

This thesis presents a comparison between a holographic model of the Pomeron in the Witten-Sakai-Sugimoto (WSS) framework and experimental data from the HERA experiment on deep inelastic scattering (DIS). The WSS model, a top-down holographic QCD dual, is utilized to describe the soft Pomeron as an exchange of glueball states. The primary focus of this work is the application of this holographic description to predict the structure functions F_1 and F_2, which characterize the DIS process at small Bjorken x. The theoretical framework builds on Regge theory and the concept of Reggeon exchange, using the Pomeron trajectory to explain the energy dependence of the cross sections. In this context, we derive the Pomeron-proton vertex, Pomeron propagator, and their coupling to photons, utilizing the tensor glueball as the leading state on the Pomeron trajectory. A key result is the derivation of the structure functions in terms of holographic parameters, which are then compared to experimental data from HERA, demonstrating a good qualitative agreement in the regime of small x and low virtuality Q^2. This work provides further insight into the use of holographic models for describing high-energy QCD processes.

Contents

Chapter 1

Introduction

The strong interaction, one of the four fundamental forces of nature, governs the behavior of quarks and gluons, the elementary particles that form protons, neutrons, and other hadrons. The widely accepted framework to describe this interaction is quantum chromodynamics (QCD). QCD, as a gauge theory based on SU(3) symmetry, describes how quarks interact by exchanging gluons. While QCD has been remarkably successful in explaining high-energy processes through perturbation theory, it presents significant challenges in its non-perturbative regime, particularly in describing phenomena such as confinement. Confinement is the property that quarks and gluons cannot be isolated and are always confined within hadrons at low energies. Despite extensive efforts, calculating QCD in this confining region remains one of the most significant unsolved problems in theoretical physics.

One promising approach to gain insights into this regime of QCD is holography, also known as the AdS/CFT correspondence. Holography provides a dual description of certain strongly coupled gauge theories in terms of weakly coupled gravitational theories in higher-dimensional spaces. Specifically, it allows the study of non-perturbative aspects of QCD using techniques from string theory and gravity. In this context, the exchange of a Pomeron, a concept originating from Regge theory, plays a pivotal role. The Pomeron is a trajectory that dominates high-energy scattering processes in QCD and is believed to represent the exchange of multiple gluons in the strong interaction. In holographic models, the Pomeron can be identified with a reggeized tensor glueball, a bound state of gluons that effectively captures the non-perturbative dynamics of QCD. This identification provides a deeper understanding of high-energy scattering processes, particularly by linking Pomeron exchange with the exchange of glueball states in the confining regime of QCD.

A key experimental process to probe the structure of hadrons is deep inelastic scattering (DIS). In this thesis, we focus on the application of holography to understand DIS in the context of Pomeron exchange. While Regge theory has been extensively used to describe the energy dependence of scattering amplitudes in the high-energy limit, holography offers a framework that unifies the soft and hard Pomeron, giving a deeper understanding of QCD in both the perturbative and non-perturbative regimes.

The aim of this work is to apply the holographic duality to study Pomeron exchange in DIS and investigate how it can provide insights into the behavior of scattering amplitudes in QCD. The central question we address is whether the holographic approach can successfully model the dynamics of QCD in the confining region, particularly through the lens of the Pomeron.

In the subsequent chapters, chapter 2 explores the principles of Regge theory. Chapter 3 investigates the theoretical framework of the soft, hard, and holographic Pomeron, elucidating their roles and interconnections within QCD. Chapter 4 focuses on the kinematics of deep inelastic scattering, establishing the foundational concepts necessary for the experimental analysis. Chapter 5 introduces the Witten-Sakai-Sugimoto (WSS) model, a pivotal holographic dual to large-N_c QCD, and discusses its application to the analysis of Pomeron exchange. Chapter 6 explores glueball states and their couplings within the holographic framework, essential for understanding the Pomeron-proton interactions. Chapter 7 presents the results of the study, including data analysis, fitting procedures, and a discussion of the implications. Finally, the appendices provide additional technical details on kinematics and scattering processes as well as supergravity.

Chapter 2

Regge Calculus

> Before the development of QCD, nobody dared to apply quantum field theory to the strong interactions
>
> J.R. Forshaw, [1]

As of today, the widely accepted theory for studying the features of the strong interaction is QCD. As is expressed in the quote above, though, physicists at first tried different ways of explaining this somewhat elusive force. The most promising way was to study the postulated properties of the $\mathcal{S}$-matrix: Lorentz invariance, unitarity and analyticity, along with the singularities required by unitarity, see appendix A and [1–5].

This framework yields a set of self-consistency conditions for scattering amplitudes. Unitarity leads to the optical theorem (see A.2), which relates the imaginary part of the forward elastic scattering amplitude to the total cross section. The requirement of analyticity leads to a dispersion relation connecting the corresponding real parts. Such a self-consistent construction is called a bootstrap, as it does not rely on any inputs from an underlying theory, such as quantum field theory (QFT). In order to make this bootstrap usable, though, one also needs to examine the asymptotic behavior of amplitudes, which is the goal of Regge theory.

2.1 Regge Theory

In this section, we will examine the basic principles of Regge theory following [1, 2, 6]. This theory has its origins in studying the features of the strong force. First attempts at describing this interaction led to the postulation of a massive particle [7], which we now know as the pion. Additionally, a plethora of particles was discovered, when examining higher-energy reactions of particles that interact through the strong force, such as neutrons and protons. Tullio Regge, therefore, established a framework in which all these seemingly different contributions of the particles involved can be described in a unified way [8].

This theoretical approach is based on the analytic properties of scattering amplitudes and the symmetries of the processes considered. The starting point is to extend the discrete integer angular momentum to continuous complex values in the radial Schrödinger equation, which can be written as

$$\psi''(x) + \left(1 - \frac{\lambda^2 - \frac{1}{4}}{x^2} - U(x)\right)\psi(x) = 0, \tag{2.1.1}$$

where $x = kr$ and λ is the generalized complex angular momentum. Physical states then correspond to half-integer values of λ with $\lambda = j + \frac{1}{2}$. This leads to the so-called *Regge trajectories* α, which are curves in the complex angular momentum plane relating the angular momentum of a particle to its mass squared. Since the angular momentum of the initial and final state in a scattering event must be conserved, equation (2.1.1) can be solved for each individual value of angular momentum separately in terms of the partial wave amplitudes. If $U(r)$ is a superposition of Yukawa potentials, the singularities of those partial wave amplitudes in the complex angular momentum plane are called *Regge poles*, which correspond to physical particles. This is an important feature, as it allows for the classification of seemingly different particles, where the relation between angular momentum and mass of the particles follows a distinct proportionality, as part of one and the same Regge trajectory.

Regge theory is valid in the so-called Regge limit, which refers to the regime of high center of mass energies and fixed momentum transfer with $s \gg |t|$ and $s \to \infty$. In this limit, the scattering amplitudes are dominated by the exchange of *Reggeons*, which are a collective name for families of particles corresponding to a specific Regge trajectory. Physical particles then coincide to integer values of angular momentum. The energy dependence of the scattering amplitude in this limit is determined by those trajectories. It can therefore be described by an exchange of a single object embodying the properties of an entire family of particles along a trajectory. Those trajectories are denoted by $\alpha(t)$, which for most purposes and standard Regge theory are assumed to be linear in t and therefore can be characterized by the slope α' and the intercept α_0 of the given trajectory. Reggeon exchange results in a characteristic energy dependence of the amplitude of the form

$$\left(\frac{s}{s_0}\right)^{\alpha(t)}. \tag{2.1.2}$$

There exist various Regge trajectories and the first ones considered were the meson trajectories. In this work, though, we are interested in a special form of Regge exchange called the *Pomeron*. This trajectory was theoretically proposed in order to explain the rise of the total pp cross-section with energy. The Pomeron has quantum numbers of the vacuum, with isospin 0 and charge conjugation parity $C = +1$ and is therefore considered to behave like a photon, except that the photon has $C = -1$. It is up to debate whether there exist two different Pomeron trajectories with different slope and intercept, which are called *soft* and *hard* Pomeron. The soft Pomeron is associated with non-perturbative QCD effects and describes the behavior of total cross-sections at lower energies, while the hard

Pomeron is linked to perturbative QCD processes and becomes significant at higher energies or in processes involving large momentum transfers. Details about the Pomeron model of Donnachie and Landshoff can be found in [9–12]. The Pomeron can also be understood as the reggeized exchange of a pair of gluons [13, 14]. In the holographic model used in the following sections, there exists only a single soft Pomeron trajectory consisting of glueball states. The lowest mass state contributing to this trajectory is a 2^{++} glueball, while the lighter 0^{++} state is only subleading [15]. For further information about the *hard* Pomeron and a holographic prescription by Brower et al., unifying both Pomeron trajectories, see chapter 3.

2.2 Regge Pole Formalism

2.2.1 Crossing Symmetry

The amplitude can be defined as a quantity only depending on the Mandelstam variables s and t, see appendix A.1 and (A.1.2). Crossing symmetry then states that $\mathcal{A}(s,t)$ can be analytically continued to the three physical regions in the Mandelstam plane. An example of this kind of symmetry is the correspondence of the amplitudes of Bhabha and Coulomb scattering, see e.g. [6].

In order to analytically continue the amplitude $\mathcal{A}(s,t)$ some assumptions about the analytic structure have to be made. One such assumption is, as was already hinted at in the introduction of this chapter, that bound states correspond to poles in the amplitude. Thresholds are connected to branch cuts and any singularity has dynamical origin (i.e. particles). A pole at $s = s_B$ with branch points and cuts corresponds to a s-plane bound state of mass $m_B = \sqrt{s_B}$ with a certain physical threshold. This correspondence stems from (A.2.4) and the optical theorem. For n particles the thresholds for production of states with masses $M_1, M_2, \dots$ is at $s = (M_1 + M_2 + \cdots)^2$, thus for equal masses they are at $s = 4m^2, 9m^2, \dots$ corresponding to the branch points of the amplitude.

With the knowledge of the analytic structure of $\mathcal{A}(s,t)$, a dispersion relation can be derived. Fixing t and integrating over a contour with a pole at $s' = s$ and $u' = u$, we get for the amplitude [4]

$$\mathcal{A}(s,t) = \frac{g_s^2}{s - s_B} + \frac{1}{2\pi i}\int_{s_0}^{\infty} ds' \frac{D_s(s',t,u')}{s' - s} + (s \leftrightarrow u), \tag{2.2.1}$$

where s_0 and u_0 are the lower thresholds for the lowest accessible states in the respective channel and $D_s(s',t,u')$ refers to the s-channel discontinuity, defined as

$$D_s(s,t,u) = -2\pi i g_s^2 \delta(s - s_B) \quad \text{for} \quad s < 4m^2. \tag{2.2.2}$$

With this (2.2.1) can be rewritten more compactly as

$$\mathcal{A}(s,t) = \frac{1}{2\pi i}\int_0^{\infty} \mathrm{d}s' \, \frac{D_s(s',t,u')}{s' - s} + \frac{1}{2\pi i}\int_0^{\infty} \mathrm{d}s' \, \frac{D_u(s',t,u')}{u' - u}, \tag{2.2.3}$$

where the discontinuities now include any bound-state contributions.

2.2.2 Partial-Wave Series Expansion

For spinless particles, the amplitude for a two-particle to two-particle scattering process at a center of mass energy of $\sqrt{s}$ much larger than the masses of the particles involved can be expanded in terms of the Legendre polynomials $P_l(\cos\theta)$ as

$$\mathcal{A}(s,t) = 16\pi \sum_{l=0}^{\infty} (2l+1)\, A_l\,(t)\, P_l\,(z_t) \tag{2.2.4}$$

with

$$z_t = \cos\theta_t = 1 + \frac{2s}{t}, \tag{2.2.5}$$

where θ_t is the scattering angle with respect to t and A_l are called the partial wave amplitudes. For $s \to \infty$ the argument of the Legendre polynomials z_t becomes proportional to s. Through crossing symmetry this statement also holds for the exchange of the two variables s and t in (2.2.4). For large z the Legendre polynomials are then proportional to z^l and we get

$$P_l\,(z_t) \sim s^l \tag{2.2.6}$$

and (2.2.4) diverges. Therefore one has to start in a region where the series converges and then analytically continue to the regions of interest. The divergence of the sum can be ignored by only considering one resonance with a given spin σ and thus only one partial wave contributes. For large s the amplitude then becomes

$$\mathcal{A}\,(s,t) = 16\pi\,(2J+1)\,A_J(t) P_J\left(1+\frac{2s}{t}\right) \sim f(t) s^J \tag{2.2.7}$$

The optical theorem then gives

$$\sigma^{tot} \sim s^{J-1} \tag{2.2.8}$$

Taking a look at particles with different spins we see the proportionality of the cross sections of particles with corresponding spins:

- **spin-0** $\sim s^{-1}$
- **spin-1** $\sim const.$
- **spin-2** $\sim s^1$

This behavior is not observed though. For low values of $\sqrt{s}$ the cross section is proportional to $s^{-0.5}$ and for higher energies it increases more slowly than expected. In order to explain the energy dependence all the resonance contributions of different spins have to combine in an appropriate way. This means that all the mesons, e.g. f_2, are members of a family of resonances with increasing spin and mass. For the right center of mass energy dependence one has to consider the family as a whole, which can be done in the Regge formalism described above.

The underlying idea of this formalism is to allow a continuous complex valued orbital angular momentum l and that the Schrödinger equation can be solved for complex l and

a spherically-symmetric potential. The partial wave amplitudes can then be considered as functions of complex l:

$$A(l,t) = A_l(t) \tag{2.2.9}$$

If the potential is a superposition of Yukawa potentials then $A(l,t)$ has poles (i.e. Regge poles) in the complex l-plane which vary with t via $l = \alpha(t)$. The $\alpha(t)$ are linear trajectories in the M^2 versus spin plane and are called Regge trajectories. Different particles may lie on the same Regge trajectory, thus families of particles can be identified by the different slopes and intercept of those trajectories. There also exist so-called *daughter* trajectories, which have the same slope, but different intercept. Although one could also consider non-linear trajectories, in our case only linear $\alpha(t)$ are of interest and thus it is sufficient to consider trajectories with

$$\alpha(t) = \alpha(0) + \alpha' t \tag{2.2.10}$$

The masses of resonances with a certain spin correspond to the values of t, where $\alpha(t)$ is a non-negative integer.

2.2.3 Sommerfeld-Watson Transform

Since the interpolation from non-negative integer values to the complex l-plane is not unique, one has to introduce even- and odd-signature amplitudes:

$$\mathcal{A}^{\pm}(l,t) = \begin{cases} A_l(t) & l \text{ even} \\ A_l(t) & l \text{ odd} \end{cases} \tag{2.2.11}$$

Then we can write (2.2.4) as

$$\mathcal{A}(s,t) = A^{+}(s,t) + A^{-}(s,t) \tag{2.2.12}$$

with

$$\mathcal{A}^{\pm}(s,t) = 8\pi \sum_{l=0}^{\infty} (2l+1)\, A_l(t) \left(P_l(z_t) \pm P_l(-z_t)\right) \tag{2.2.13}$$

Considering that $\frac{1}{\sin(\pi l)}$ has poles at non-negative integer values of l the series can be rewritten as a Cauchy integral over the l-plane, where the amplitudes are analytic on the right-hand half with only isolated singularities:

$$\mathcal{A}^{\pm}(s,t) = 8\pi \int_C dl\, (2l+1)\, A^{\pm}(l,t)\, \frac{P_l(z_t) \pm P_l(-z_t)}{\sin(\pi l)} \tag{2.2.14}$$

Moving the contour of this integral from $+\infty$ to the left means that we have to integrate around all the poles $\alpha_i^{\pm}(t)$ and pick up their residues $\beta_i^{\pm}(t)$ until $\operatorname{Re} l = -\frac{1}{2}$. The result is then

$$\begin{aligned} \mathcal{A}^{\pm}(l,t) = &-16\pi^2 \sum_i \frac{\left(2\alpha_i^{\pm}(t)+1\right)\beta_i^{\pm}(t)}{\sin\left(\pi\alpha_i^{\pm}(t)\right)} \left(P_{\alpha_i^{\pm}(t)}(-z_t) \pm P_{\alpha_i^{\pm}(t)}(z_t)\right) \\ &+ 8\pi \int_{-\frac{1}{2}-i\infty}^{-\frac{1}{2}+i\infty} \mathrm{d}l\, \frac{(2l+1)\, A^{\pm}(t)}{\sin(\pi l)} \left(P_l(-z_t) \pm P_l(z_t)\right) \end{aligned} \tag{2.2.15}$$

where the integral is the so called background integral and is not of interest for our discussion. With the identity $P_l(z) = e^{-i\pi l} P_l(-z)$ for large negative z we can rewrite the factor outside the fraction as $\left(1 \pm e^{-i\pi\alpha_i^{\pm}(t)}\right) P_l(-z)$ where the factors in parentheses are the signature factors $\xi_\alpha^{\pm}$ which determine the phase of the high-energy behavior of Regge-pole contributions to the amplitude.

Using the asymptotic behavior of the Legendre polynomials

$$P_\alpha(z) \sim \frac{\Gamma\left(\alpha + \frac{1}{2}\right)}{\Gamma\left(\alpha + 1\right)} (2z)^\alpha , \tag{2.2.16}$$

the properties of the Γ-function

$$l\Gamma(l) = \Gamma(l+1) \tag{2.2.17}$$

and

$$\Gamma(l+1)\Gamma(-l) = -\frac{\pi}{\sin(\pi l)} \tag{2.2.18}$$

and the redefinition of the residues $\beta_i^{\pm}(t)$ by absorption of unwanted factors, the amplitudes have the leading behavior

$$\mathcal{A}^{\pm}(s,t) \sim \sum_i \beta_i^{\pm}(t)\Gamma\left(-\alpha_i^{\pm}(t)\right)\left(1 \pm e^{-i\pi\alpha_i^{\pm}(t)}\right) s^{\alpha_i^{\pm}(t)}. \tag{2.2.19}$$

Most of the time it is beneficial to get rid of the mass dimension of s via relating it to some scale s_0 and make the replacement $s \to \left(\frac{s}{s_0}\right)$, since dimensionful quantites are not to be potentiated.

The odd- and even-signatured amplitudes then depend on the values where the $\Gamma\left(\alpha_i^{\pm}(t)\right)$ have poles and we can identify these poles with the exchanges of particles with even or odd spin $\sigma^{\pm}$, whose squared mass is the corresponding value of t.

Chapter 3

Soft, Hard, and Holographic Pomeron

For general remarks on holographic QCD and the connection to Regge theory, see [16] and [17, 18], where the latter also includes a general discussion of deeply virtual Compton scattering (DVCS) in a holographic dual of 5d string theory. In this section, though, we will follow the discussion as presented in [19, 20]. For further information about bottom-up models of holographic QCD, see e.g. [21].

3.1 The Pomeron and the Duality

Applying Regge theory to DIS was necessary in order to describe the behavior of cross sections as presented in (2.2.8). The trajectory of the Pomeron has an intercept of around 1.08, which was found to depend on the virtuality of the off-shell photon Q^2. For higher values of Q^2 the observed intercept rises to 1.4, suggesting another trajectory, leading to the distinction between the non-perturbative *soft* and the perturbative *hard* or Balitsky-Fadin-Kuraev-Lipatov (BFKL) Pomeron, where the former was already introduced in the first section. Both objects share the same quantum numbers, but refer to different entities as they most notably differ in their value of the intercept. In the following sections we will introduce the BFKL Pomeron, explain the conceptual differences to the soft Pomeron presented before, discuss a holographic approach, aiming to unify the descriptions, as well as compare it to the way the Pomeron is used in our discussion.

3.2 Perturbative Pomeron

In QCD it is not straightforward to construct an object such as the Pomeron from scratch. As was pointed out before, the Pomeron has the quantum numbers of the vacuum and therefore also needs to be a color-singlet object. Candidates for the fundamental particles making up the Pomeron are therefore gluons and in the approach of BFKL, an infinite set of gluon ladder diagrams are summed. In the following sections we will present the

initial considerations for constructing this elusive trajectory and will focus on the concepts and ideas behind this construction, rather than the mathematical rigor behind it. The full description of this approach can be found in [1, 5].

3.2.1 The Reggeized Gluon

The first process to consider is the scattering of two massless quarks of different flavors due to colour octet exchange within the Regge limit. Using the eikonal approximation (i.e. all q^μ components are small compared to the components of p_i^μ for $s \gg |t|$), the upper quark line of this Feynman diagram can be written as

$$-2igp_1^\mu \tau_{ij}^a, \tag{3.2.1}$$

with the generators of the colour group in the fundamental representation τ_{ij}^a. Also note that we dropped the factors of $\delta_{\lambda_1'\lambda_1}$, which ensures helicity conservation. Approximating the lower vertex similarly, the lowest order amplitude for this type of scattering is then given by

$$\mathcal{A}^{(0)} = 8\pi\alpha_s \frac{s}{t} \tau_{ij}^a \tau_{kl}^a, \tag{3.2.2}$$

where $\alpha_s = \frac{g^2}{4\pi}$ is the strong coupling constant.

In next to leading order $\mathcal{O}(\alpha_s)$ the Feynman diagrams of interest are the box and crossed box two-gluon exchange diagrams. Diagrams with self-energy insertions on the other hand are only subleading in $\ln s$ and therefore can be ignored. Since these diagrams determine the renormalization of the coupling constant, this also means that from this point on, we are fixing α_s to be constant, which has to be remedied later in the discussion. Scattering amplitudes are most efficiently calculated using the so-called Cutkosky rules, from which the imaginary part of the amplitudes can be obtained via cutting the quark lines as

$$\operatorname{Im} \mathcal{A}^{(1)} = \frac{1}{2} \int \mathrm{d}\Pi_2 \, \mathcal{A}^{(0)}\big(s, k^2\big) \mathcal{A}^{(0)\dagger}\big(s, (k-q)^2\big), \tag{3.2.3}$$

with the two-body phase space given by

$$\int \mathrm{d}\Pi_2 = \int \frac{\mathrm{d}^4 k}{2\pi^2} \delta\big((p_1 - k)^2\big) \delta\big((p_2 + k^2)\big) = \frac{1}{8\pi^2 s} \int \mathrm{d}^2\mathbf{k}\,. \tag{3.2.4}$$

With (3.2.2) we therefore get

$$\mathcal{A}^{(0)}\big(s, k^2\big) = -8\pi\alpha_s \tau_{mj}^a \tau_{nl}^a \frac{s}{\mathbf{k}^2} \tag{3.2.5}$$

$$\mathcal{A}^{(0)\dagger}\big(s, (k-q)^2\big) = -8\pi\alpha_s (\tau_{mi}^a \tau_{nk}^a)^* \frac{s}{(\mathbf{k}-\mathbf{q})^2}. \tag{3.2.6}$$

Using the leading logarithmic expansion [22] yields for the amplitude

$$\mathcal{A}_{\text{box}}^{(1)} = -\frac{16\pi\alpha_s^2}{N_c} \frac{s}{t} (\tau^a\tau^b)_{ij} (\tau^a\tau^b)_{kl} \ln\Big(\frac{s}{t}\Big) \epsilon(t), \tag{3.2.7}$$

with

$$\epsilon(t) = \frac{N_c \alpha_s}{4\pi^2} \int \mathrm{d}^2\mathbf{k}^2 \, \frac{-\mathbf{q}^2}{\mathbf{k}^2(\mathbf{k}-\mathbf{q})^2}, \tag{3.2.8}$$

where $\epsilon(t)$ is related to the trajectory of the reggeized gluon as

$$\alpha_g(t) = 1 + \epsilon(t). \tag{3.2.9}$$

The integral in (3.2.8) is infrared divergent, because the external quarks are on mass-shell. Therefore an infrared cutoff has to be introduced, taking into account the off-shellness of the confined quarks.

The contribution of the crossed box diagram is simply given by replacing s with u, using $u \simeq -s$ and acknowledging the change of the color factors

$$\mathcal{A}^{(1)}_{\text{crossed}} = \frac{16\pi\alpha_s^2}{N_c} \frac{s}{t} (\tau^a\tau^b)_{ij} (\tau^b\tau^a)_{kl} \ln\left(\frac{s}{t}\right) \epsilon(t). \tag{3.2.10}$$

Contracting the color factors then yields

$$\mathcal{A}^{(1)} = 8\pi\alpha_s \frac{s}{t} \tau^a_{ij}\tau^a_{kl} \ln\left(\frac{s}{t}\right) \epsilon(t) = \mathcal{A}^{(0)} \ln\left(\frac{s}{t}\right) \epsilon(t). \tag{3.2.11}$$

For higher order terms, diagrams with an additional gluon have to be taken into account, i.e. $qq \to qq + g$. To do so, a gauge invariant non-local effective vertex $\Gamma^\sigma_{\mu\nu}(\mathbf{k}_1, \mathbf{k}_2)$ is introduced. The amplitude in leading logarithmic approximation up to order α_s^2 is then given by

$$\mathcal{A}^{(0)} \left(1 + \epsilon(t) \ln\left(\frac{s}{\mathbf{k}^2}\right) + \frac{1}{2}\epsilon^2(t) \ln^2\left(\frac{s}{\mathbf{k}^2}\right) + \dots\right), \tag{3.2.12}$$

where the term in parenthesis simply resembles a Taylor expansion of the expression $\left(\frac{s}{t}\right)^{\epsilon(t)}$, implying the ansatz

$$\mathcal{A} = \mathcal{A}^{(0)} \left(\frac{s}{t}\right)^{\epsilon(t)}, \tag{3.2.13}$$

which introduces the reggeized gluon propagator

$$D_{\mu\nu}(s, q^2) = -i \frac{g_{\mu\nu}}{q^2} \left(\frac{s}{s_0}\right)^{\epsilon(q^2)}, \tag{3.2.14}$$

cp. (2.1.2). Extending the ideas presented above to even higher orders, i.e. $qq \to qq + n$ gluons, leads to the so-called BFKL ladder, where all the vertical lines are reggeized gluons.

3.2.2 BFKL Equation

Calculating the amplitude for this type of multi-Regge exchange then yields the BFKL equation [1, 5], which is used to describe the leading logarithmic evolution in $\ln s$ of the gluon ladder. In the case of $t = 0$, this integral equation can be solved by finding the eigenfunctions and corresponding eigenvalues of the so-called BFKL kernel $\mathcal{K}_0$. By taking a closer look at the gluon ladders themselves, one finds that the scale of typical transverse momenta involved is entirely set by the impact factors, which determine the coupling of

the Pomeron to hadrons, at the top and the bottom of the ladder. Since the BFKL equation is infrared safe, the integrations over transverse momenta must be dominated by the horizontal momenta $\mathbf{k}_h$. But when going further away from the ends of the ladder, where $\mathbf{k}_h$ is set, more and more momenta become significant and in this way the running of the coupling is introduced into the BFKL framework. This behavior of the broadening of the momentum range can be understood as a diffusion effect. This type of diffusion can also be found from a holographic point of view, see section 3.4.1.

3.3 Soft versus Hard Pomeron

The description of the perturbative Pomeron presented in this section is quite different from the soft Pomeron. They most notably differ in their value of the intercept. The hard intercept is found by solving the BFKL equation and the soft intercept via experimental observations to be

$$\alpha_{\text{hard}}(0) = 1 + \alpha_s N_c \frac{4\ln 2}{\pi}\bigg|_{\alpha_s=0.2} \simeq 1.5 \quad \text{and} \quad \alpha_{\text{soft}}(0) \simeq 1.08. \tag{3.3.1}$$

There exists two different points of view in treating this discrepancy. On the one hand, the soft and hard Pomeron are considered to be two distinct objects. The soft Pomeron then would inherently describe the non-perturbative region and the hard Pomeron the large $|t|$ region, becoming irrelevant as Q^2 goes to zero. On the other hand, it could be the case that there exists only one Pomeron and the intercept is actually Q^2 dependent, interpolating between the soft and the hard case. One specific way of treating the Pomeron in this manner will be presented in the following section.

As a concluding remark for the BFKL Pomeron it has to be noted that this description failed to satisfy its original purpose, namely to calculate perturbatively the rapid rise of $\sigma^{\gamma^* p}$ with W^2 at small x, parameterized as an effective power

$$\sigma^{\gamma^* p} \approx F(Q^2)(W^2)^{\lambda(Q^2)}. \tag{3.3.2}$$

However, the calculations of BFKL are considered to be almost certainly invalid. The approximations used to derive the BFKL equation do not take into account energy conservation in a suitable manner and also fail to incorporate non-perturbative effects such as confinement [1, 5]. Nonetheless, there are ongoing efforts to include confinement in the BFKL framework, such as introducing modifications to the BFKL kernel [23].

3.4 Holographic Pomeron

Following [19], this section aims to present yet another formulation of the Pomeron and its properties. The motivation behind this new description has already been mentioned before: How are the *soft* and *hard* Pomeron related? What is the connection between the tensor glueball exchange on one hand and the exchange of a ladder of reggeized gluons on the other? Brower et al. try to solve this problem in a holographic manner. They

do so by using concepts of string theory in curved-space and are able to find a single j-plane Schrödinger operator, interpolating between the two descriptions, unifying the BFKL Pomeron at negative t and the *soft* Pomeron at positive t.

In the Regge regime ($s \to \infty$, t fixed) the Regge behavior of QCD amplitudes is in good correspondence with the scattering in string theory on flat spaces. In other regimes, this statement does not hold. For elastic scattering at large angles, for example, the amplitudes in string theory are suppressed exponentially, whereas in QCD, they are suppressed by powers of s. In order to tackle this problem, one can take a look at the limit of $N \to \infty$ and $s \to \infty$, where the scattering amplitudes are dominated by the single Pomeron exchange. As was already pointed out before, the Pomeron is a color-singlet state built from gluons. In string theory the Pomeron is identified as the Regge trajectory of the higher-dimensional graviton.

Approaching QCD in a holographic manner also has its caveats. For example, only large-N gauge theories have a small or zero beta-function and are therefore conformally invariant, which is not the case for real QCD. Also, as is the case for the BFKL framework, confinement effects are generally neglected. In holography, though, this problem can be remedied by considering different background geometries.

3.4.1 Conformally-invariant Scattering

Following the methods as presented in the previous section in the large-N limit one can write down the single-Pomeron-exchange amplitude for quarkonium states as

$$\int \frac{\mathrm{d}k_h}{k_h} \int \frac{\mathrm{d}k'_h}{k'_h} \Phi_A(k_h) \mathcal{K}\big(k_h, k'_h, s\big) \Phi\big(k'_h\big), \tag{3.4.1}$$

with the impact factors Φ_i, the magnitude of the transverse momenta $\mathbf{k}_h$ and the BFKL kernel $\mathcal{K}$. The kernel can be approximated by a diffusion kernel times a power of s as

$$\mathcal{K}\big(k_h, k'_h, s\big) \approx \frac{s^{j_0}}{\sqrt{4\pi \mathcal{D} \ln s}} e^{\frac{-\left(\ln k'_h - \ln k_h\right)^2}{4\mathcal{D} \ln s}}, \tag{3.4.2}$$

with $j_0 = 1 + \alpha_s N_c \frac{4 \ln 2}{\pi}$, cf. 3.3.1, and $\mathcal{D} = \alpha_s N_c \frac{7\zeta(3)}{2\pi}$, where the diffusion occurs in the variable $\ln k_h$ over the diffusion time $\tau \sim \ln s$. From the string theoretical point of view, this diffusion can be interpreted as a time-dilation of the boosted string, making the string appear longer and larger. This growth corresponds to a random walk in the transverse dimensions to the motion of the string.

Assuming that the holographic principle holds, the scattering of states in $\mathcal{N} = 4$ supersymmetric Yang-Mills theory is equivalent to string scattering on a curved background of the form $\mathrm{AdS}_5 \times \mathrm{S}_5$. The AdS_5 coordinates are x^μ and the holographic coordinate r of the Poincaré patch, running from $r = 0$ to $r = \infty$ at the boundary. Since the holographic coordinate can be interpreted as the energy scale of the system, $r = 0$ corresponds to the infrared and $r \to \infty$ to the ultraviolet. For $t = 0$ the scattering of two strings in such a

background can be described via

$$\mathcal{K}(r, r', s) = \frac{s^{j_0}}{\sqrt{4\pi}\mathcal{D}\ln s} e^{\frac{-(\ln r - \ln r')^2}{4\mathcal{D}\ln s}}, \tag{3.4.3}$$

with

$$j_0 = 2 - \frac{2}{\sqrt{\lambda}} + \mathcal{O}(\lambda^{-1}), \qquad \mathcal{D} = \frac{1}{2\lambda} + \mathcal{O}(\lambda^{-1}) \tag{3.4.4}$$

and the 't Hooft coupling $\lambda \equiv \frac{R^4}{\alpha'^2} = g_{YM}^2 N$, where R is the radius of the AdS_5 space. Comparing this to (3.4.2) identifies the transverse momentum of the gauge theory with the coordinate r from holography. In this sense, holography provides a promising framework for investigating the duality between gauge theory and string theory, with QCD as a specific example.

Chapter 4

Deep Inelastic Scattering

4.1 Deep Inelastic Lepton-Proton Scattering

In this section, we introduce the necessary kinematics of the reactions of interest. We will mostly follow [24–26]. Generally speaking, we are interested in DIS of charged leptons off fixed targets (protons). Only the direction and energy of the scattered leptons are measured by the detector, so we do not observe the final hadronic state. The main quantities of interest are the structure functions, which are given by the absorptive part of the forward virtual Compton amplitude. Via the optical theorem, this amplitude is related to the total cross section, see figure 4.1. The structure functions behavior at low Bjorken-x or high energy has been a research area with extensive experimental and theoretical studies in the past, e.g. [24, 27–32]. In the scope of this work, we will only be interested in aspects based on Regge theory, where the region of low-x is dominated by Pomeron exchange, see (4.2.1).

We focus on the first-order amplitude, or in other words, the first Born approximation, where only a single photon is exchanged, see figure 4.2.

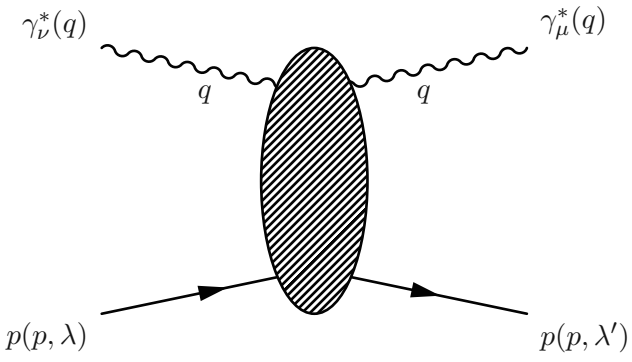

Figure 4.1. Feynman diagram of virtual Compton forward scattering.

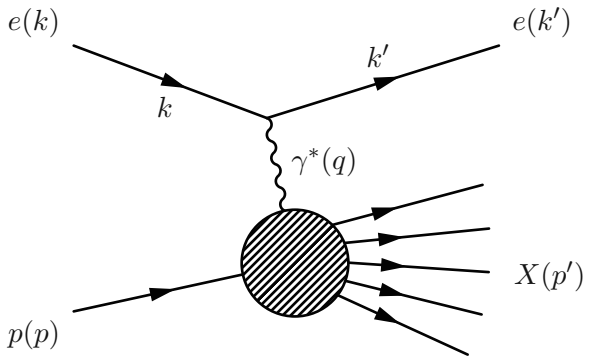

Figure 4.2. Feynman diagram for deep inelastic lepton-hadron scattering via the exchange of a virtual photon with momentum q. Since the final state is not directly measured it is denoted by X with momentum p'.

4.2 Kinematics

The process we are considering is inelastic scattering of electrons and positrons off protons, see figure 4.1. We will use the standard kinematic variables, see e.g. [25, 26, 33]. They are defined[1] as follows:

$$\begin{aligned} s &= (p+k)^2\,, \\ q &= k - k', \\ W^2 = p'^2 &= (p+q)^2\,, \\ Q^2 &= -q^2, \\ \nu = E - E' = \frac{p\cdot q}{m_p} &= \frac{W^2+Q^2-m_p^2}{2m_p}, \\ x = \frac{-q^2}{2m_p\nu} &= \frac{Q^2}{W^2+Q^2-m_p^2}, \\ y = \frac{\nu}{E} = \frac{p\cdot q}{p\cdot k} &= \frac{W^2+Q^2-m_p^2}{s-m_p^2}. \end{aligned} \tag{4.2.1}$$

Here, s is the square of the center-of-mass energy of the whole system, whereas W^2 is the square of the center-of-mass energy of the hadronic part. The quantities ν, y, x are the energy loss of the lepton, the fractional energy loss of the lepton and the Bjorken-x, respectively. We also have

$$\epsilon = \frac{2\,(1-y) - y^2\delta\left(W^2,Q^2\right)}{1+(1-y)^2+y^2\delta\left(W^2,Q^2\right)} \tag{4.2.2}$$

where

$$\delta\left(W^2,Q^2\right) = \frac{2m_p^2Q^2}{\left(W^2+Q^2-m_p^2\right)^2} \tag{4.2.3}$$

[1] Note: in holography, the mostly-plus convention is usually favored over the mostly-minus convention, cf. A.1

and the kinematic limits for y and ϵ at given $W^2 > m_p^2$ and $q^2 \leq 0$:

$$1 \geq \epsilon \geq 0 \qquad \Longleftrightarrow \qquad 0 \leq y \leq \frac{2}{1+\sqrt{1+2\delta\left(W^2, Q^2\right)}} \tag{4.2.4}$$

4.3 Deep Inelastic Scattering Amplitude

For the definition of the scattering amplitude, we will follow [25], which gives a slightly different definition compared to that of Britzger et al. [24]. The Feynman diagram for DIS is shown in figure 4.2 and the scattering amplitude for this diagram is given by

$$i\mathcal{M} = (-ie)^2 \left(\frac{-i\eta_{\mu\nu}}{q^2}\right) \langle k'|j_\ell^\mu(0)|k, s_\ell\rangle \langle X|j_h^\nu(0)|p, \lambda\rangle \,, \tag{4.3.1}$$

where $-ie$, j_ℓ and j_h are the vertex factor for both vertices, the leptonic and the hadronic electromagnetic current, respectively. The spin of the lepton and the helicity of the hadron are given by s_ℓ and λ, respectively. $\left(\frac{-i\eta_{\mu\nu}}{q^2}\right)$ is the photon propagator, where the metric stems from the sum over the polarization states of the photon[2] as [35]

$$\sum_p \varepsilon_\mu^p \varepsilon_\nu^{p*} = -\eta_{\mu\nu}. \tag{4.3.2}$$

The differential cross-section is then obtained by squaring $\mathcal{M}$, multiplied with the phase space factors and summing over the final lepton and hadron polarisation states as

$$\begin{aligned} \mathrm{d}\sigma &= \sum_X \int \frac{\mathrm{d}^3k'}{(2\pi)^3 2E'} (2\pi)^4 \delta^4\left(k + p - k' - p_X\right) \frac{|\mathcal{M}|^2}{(2E)(2M)} \\ &= \sum_X \int \frac{\mathrm{d}^3k'}{(2\pi)^3 2E'} \frac{(2\pi)^4 \delta^4(k + p - k' - p_X)}{(2E)(2M)} \frac{e^4}{q^4} \\ &\qquad \times \langle p, \lambda|j_h^\nu(0)|X\rangle \langle X|j_h^\nu(0)|p, \lambda\rangle \, \langle k, s_\ell|j_{\ell\mu}(0)|k'\rangle \langle k'|j_{\ell\nu}(0)|k, s_\ell\rangle \,. \end{aligned} \tag{4.3.3}$$

It is then instructive to define the leptonic tensor $\ell_{\mu\nu}$ as

$$\ell^{\mu\nu} = \sum_{\text{final spin}} \langle k'|j_\ell^\nu(0)|k, s_\ell\rangle \langle k, s_\ell|j_\ell^\mu(0)|k'\rangle \,, \tag{4.3.4}$$

as well as the hadronic tensor $W_{\mu\nu}$ as

$$W^{\mu\nu}(p,q)_{\lambda\lambda'} = \frac{1}{4\pi} \int \mathrm{d}^4x \, e^{iq\cdot x} \left\langle p, \lambda'\middle|\left[j_h^\mu(x), j_h^\nu(0)\right]\middle|p, \lambda\right\rangle \,, \tag{4.3.5}$$

with the polarisations of the initial and final hadron λ and λ'. The commutator is only needed for analytic continuation and is of no interest for the process given here, as can be seen in the following. Inserting a complete set and exploiting translation invariance yields

$$\begin{aligned} W^{\mu\nu}(p,q)_{\lambda\lambda'} = \frac{1}{4\pi} \sum_X \Big[&(2\pi)^4 \delta^4(q + p - p_X) \, \langle p, \lambda'|j_h^\mu(0)|X\rangle \langle X|j_h^\nu(0)|p, \lambda\rangle \\ &- (2\pi)^4 \delta^4(q + p - p_X) \, \langle p, \lambda'|j_h^\nu(0)|X\rangle \langle X|j_h^\mu(0)|p, \lambda\rangle \Big]. \end{aligned} \tag{4.3.6}$$

[2] At this stage of the discussion, we are only considering the leptonic current. Due to the gauge freedom of QED [3, 34], it is sufficient to consider the polarization sum as in (4.3.2). In general, for a massive off-shell photon, one needs to consider the polarizations as presented in (4.7.1) and (7.1.1).

Since the only allowed states are those with $p_X^0 \geq p^0$, only the first term survives and the commutator in (4.3.5) can be dropped.

4.4 Double Virtual Forward Compton Scattering

In DIS, one effectively studies the absorption of the virtual photon on the proton as depicted in figure 4.1. Since the total $\gamma^* p$ absorption cross section is related to the absorptive part of the virtual forward Compton scattering amplitude, we will focus on this scattering process given by

$$\gamma^*(q) + p(p,\lambda) \longrightarrow \gamma^*(q) + p(p,\lambda') \tag{4.4.1}$$

and figure 4.1. Using a different notation from Britzger et al., the amplitude is given by

$$\mathcal{T}^{\mu\nu} = i \int \mathrm{d}^4x \, e^{iq\cdot x} \left\langle p,\lambda' \middle| \hat{T}(j^\mu(x) j^\nu(0)) \middle| p,\lambda \right\rangle , \tag{4.4.2}$$

where $\hat{T}$ denotes the covariantised time-order product and $j^\mu(x)$ the hadronic part of the electromagnetic current. Comparing this quantity to (4.3.5) we see that $\mathcal{T}^{\mu\nu}$ and $W^{\mu\nu}$ share the same structure and therefore can be decomposed in an equivalent way. Using the optical theorem mentioned before we have

$$\sum_X \int \mathrm{d}LIPS \, |\mathcal{T}_{\gamma p \to X}|^2 = 2 \operatorname{Im} \mathcal{T}_{\gamma p \to \gamma p}(s, t=0) \tag{4.4.3}$$

and one therefore gets the relations

$$2 \operatorname{Im} \mathcal{T}^{\mu\nu} = 4\pi W^{\mu\nu} \tag{4.4.4}$$

and we therefore define the hadronic tensor in an equivalent way as

$$W^{\mu\nu}_{\lambda\lambda'} = \frac{i}{2\pi} \int \mathrm{d}^4x \, e^{iq\cdot x} \left\langle p,\lambda' \middle| \hat{T}(j^\mu(x) j^\nu(0)) \middle| p,\lambda \right\rangle . \tag{4.4.5}$$

4.5 Form Factors

For any particle that interacts with quarks confined within a hadron, so-called form factors have to be introduced. They aim to capture our ignorance of certain properties about the scattered particles. Since the Pomeron can be seen as a $C = 1$ photon, it is reasonable to introduce two form factors, the Dirac and Pauli form factors $F_1(t)$ and $F_2(t)$, respectively and it is assumed that they are equal for $C = 1$ and $C = -1$. F_2 takes into account that quarks are not free when scattered, but bound within hadrons. Since the Pomeron is an isosinglet exchange, the Pauli form factor includes the elastic electromagnetic form factor of the proton and the neutron. At $t = 0$, F_2 can be omitted, as the value of this form factor is merely the sum of the anomalous magnetic moments of the proton and the neutron, which is small and also remains small for $t > 0$. F_1, on the other hand, is only determined by the proton form factor, since the one for the neutron is negligibly small.

4.6 Hadronic Tensor and Structure Functions

As mentioned in the section 4.4, the hadronic tensor is defined as the absorptive part of $\mathcal{T}^{\mu\nu}_{\lambda'\lambda}$, averaged over the proton helicities. For reference, we will start with giving the definitions as presented in [24]:

$$W^{\mu\nu}(p,q) = \frac{1}{2}\sum_{\lambda',\lambda}\delta_{\lambda'\lambda}\frac{1}{2i}\left[\mathcal{T}^{\mu\nu}_{\lambda'\lambda}(p,q) - \left(\mathcal{T}^{\nu\mu}_{\lambda'\lambda}(p,q)\right)^*\right]. \tag{4.6.1}$$

Focusing on the unpolarized case, this tensor can also be expressed using the structure functions of DIS, W_1 and W_2:

$$\begin{aligned} W^{\mu\nu}(p,q) = {} & W_1\left(\nu,-q^2\right)\left(-\eta^{\mu\nu}+\frac{q^\mu q^\nu}{q^2}\right) \\ & -\frac{1}{m_p^2}W_2\left(\nu,-q^2\right)\left(p^\mu-\frac{p\cdot q}{q^2}q^\mu\right)\left(p^\nu-\frac{p\cdot q}{q^2}q^\nu\right). \end{aligned} \tag{4.6.2}$$

We will also need the transverse and longitudinal cross sections for the total $\gamma^* p$ absorption process defined as

$$\begin{aligned} \sigma_T\left(W^2,-q^2\right) &= \frac{2\pi m_p}{W^2-m_p^2}e^2 W_1\left(\nu,Q^2\right) \\ \sigma_L\left(W^2,-q^2\right) &= \frac{2\pi m_p}{W^2-m_p^2}e^2\left[W_2\left(\nu,Q^2\right)\frac{\nu^2+Q^2}{Q^2}-W_1\left(\nu,Q^2\right)\right] \end{aligned} \tag{4.6.3}$$

where $e>0$ is the proton charge. In the following though, we will make use of the dimensionless structure functions $F_1 = W_1$ and $F_2 = -\frac{\nu}{m_p}W_2$, with the definitions presented in the section above and rewrite (4.6.1) as

$$W^{\mu\nu}(p,q) = \frac{1}{2}\sum_{\lambda,\lambda'}\delta_{\lambda\lambda'}\,\mathrm{Im}\,\mathcal{T}^{\mu\nu}_{\lambda\lambda'}(p,q) = \frac{1}{2i}\sum_{\lambda,\lambda'}\left[\mathcal{T}^{\mu\nu}_{\lambda\lambda}(p,q) - \mathcal{T}^{*\nu\mu}_{\lambda\lambda}(p,q)\right], \tag{4.6.4}$$

(4.6.2) as

$$\begin{aligned} W^{\mu\nu}(p,q) = {} & F_1(x,q^2)\left(-\eta^{\mu\nu}+\frac{q^\mu q^\nu}{q^2}\right) \\ & +\frac{2x}{q^2}F_2(x,q^2)\left(p^\mu+\frac{q^\mu}{2x}\right)\left(p^\nu-\frac{q^\nu}{2x}\right) \end{aligned} \tag{4.6.5}$$

and (4.6.3) as

$$\begin{aligned} \sigma_T\left(q^2,\nu\right) &= \frac{4\pi^2\alpha_{em}}{m_p\kappa_\gamma}F_1\left(q^2,\nu\right) \\ \sigma_L\left(q^2,\nu\right) &= \frac{4\pi^2\alpha_{em}}{m_p\kappa_\gamma}\left[-F_1\left(q^2,\nu\right)+\frac{m_p}{\nu}\left(q+\frac{\nu^2}{q^2}\right)F_2\left(q^2,\nu\right)\right], \end{aligned} \tag{4.6.6}$$

where $e^2 = 4\pi\alpha_{em}$ and the flux factor in Hand's convention $\kappa_\gamma = \nu - \frac{q^2}{2m_p}$, cf. [36], which normalizes the flux of incoming particles.

The quantity that is directly measured at HERA is the reduced cross section defined as

$$\begin{aligned}\sigma_{\text{red}}\big(q^2, W^2, y\big) = &\frac{1+(1-y)^2+y^2\delta\big(W^2,q^2\big)}{\Big(1+(1-y)^2\Big)\big(1+2\delta(W^2,q^2)\big)}\frac{q^2}{4\pi^2\alpha_{em}}(1-x)\\ &\times\big[\sigma_T\big(W^2,q^2\big)-\varepsilon\sigma_L\big(W^2,q^2\big)\big]\end{aligned} \tag{4.6.7}$$

and the total photoproduction cross section is given by

$$\sigma_{\gamma p}\big(W^2\big) = \sigma_T\big(W^2,0\big). \tag{4.6.8}$$

4.7 Matrix Element for Pomeron Scattering

For large W^2, small x, the virtual Compton amplitude is deemed to be dominated by the exchange of soft and hard Pomerons, as well as the f_{2R} reggeon, in the case of the tensor-Pomeron approach of Britzger et al. In our approach, we are only considering the contribution of one Pomeron and no other reggeons, therefore restricting to low Q^2 as well as low-x. Our expression for the matrix element will look similar to that presented there, but our definitions of the quantities used, such as the Pomeron propagator and the Pomeron-proton-proton vertex, will be different. Also, since we are dealing with off-shell photons, we need to take into account the polarization terms. For the matrix element we find

$$\mathcal{T}^{\mu\nu}_{\lambda\lambda'} = \frac{1}{i2\pi m_p e^2}\left(-\eta^{\mu\alpha}+\frac{q^\mu q^\alpha}{q^2}\right)\left(-\eta^{\nu\sigma}+\frac{q^\nu q^\sigma}{q^2}\right) i\mathbb{V}_{\alpha\beta\kappa\lambda} i\Delta^{\kappa\lambda,\gamma\delta} i\Gamma_{\gamma\delta}, \tag{4.7.1}$$

with

$$\Gamma^{\mathcal{G}pp}_{\mu\nu} = \lambda_{\mathcal{P}}\left(\bar{u}\big(p',s'\big)\frac{\gamma_\mu P_\nu+\gamma_\nu P_\mu}{2}u(p,s)\right) \tag{4.7.2}$$

$$\begin{aligned}\mathbb{V}^{\alpha\beta\kappa\lambda} = &\, e^2\,\mathrm{Tr}\big(\mathcal{Q}^2\big)\left[\frac{t_2 q^4}{M_{KK}^2}\Big(\eta^{\alpha\kappa}\eta^{\beta\lambda}+\eta^{\beta\kappa}\eta^{\alpha\lambda}\Big)\right.\\ &+t_3\Big(\eta^{\beta\lambda}q^\kappa q^\alpha+\eta^{\alpha\lambda}q^\kappa q^\beta+\eta^{\alpha\kappa}q^\beta q^\lambda+\eta^{\beta\kappa}q^\alpha q^\lambda\\ &\left.-2\eta^{\alpha\beta}q^\kappa q^\lambda-q^2\Big(\eta^{\alpha\kappa}\eta^{\beta\lambda}+\eta^{\beta\kappa}\eta^{\alpha\lambda}\Big)\Big)\right]\end{aligned} \tag{4.7.3}$$

$$\Delta^{\mathcal{G}}_{\mu\nu,\gamma\delta} = \frac{1}{2s}\left(\eta_{\alpha\gamma}\eta_{\beta\delta}+\eta_{\beta\gamma}\eta_{\alpha\delta}-\frac{1}{2}\eta_{\alpha\beta}\eta_{\gamma\delta}\right)\big(-i\alpha'_{\mathcal{G}}s\big)^{\epsilon_{\mathcal{G}}}, \tag{4.7.4}$$

see (6.5.4), (6.6.9) and (6.6.23). From these expressions, the matrix element can be calculated, allowing the structure functions W_1 and W_2 to be determined by comparison with equation (4.6.2).

Chapter 5

Witten-Sakai-Sugimoto Model

In this section, the model of Sakai and Sugimoto [37, 38], which is a holographic dual to large N_c QCD with massless flavors in four dimensions, will be presented. It is often also called the WSS model, acknowledging the important work of Edward Witten [39] regarding the AdS-structure, thermal phase transition and confinement in holographic theories. Following [37, 38], this model is constructed by placing N_f probe flavor D8-branes into a D4-brane background consisting of N_c color branes. We demand $N_f \ll N_c$ and therefore the high N_c limit ensures that the flavor branes can be introduced as a probe, so that the back-reaction of those branes on the color brane background is negligible. In principle, these could be considered as well, but it can be rather challenging and for the scope of this discussion, no deeper insight is to be expected by doing so. The background of the WSS model satisfies the supergravity equations of motion in ten dimensions, see appendix B.

Other top-down models, e.g. [40], using D6-branes in a D4 background, fail to contain the spontaneous breaking of chiral symmetry in QCD and therefore do not produce the massless pions as Nambu-Goldstone bosons of this symmetry. In order to implement the breaking of supersymmetry and the spontaneous breaking of the $U(N_f)_L \times U(N_f)_R$ chiral symmetry into this model, the configuration of the branes is crucial. SUSY is broken by compactifying the N_c D4-branes on a S^1 of radius M_{KK}^{-1} as well as imposing antiperiodic boundary conditions for the fermions on those branes. The chiral symmetry is broken by placing N_f D8 $-$ $\overline{\text{D8}}$ pairs transversely to this S^1:

	0	1	2	3	4	5	6	7	8	9
D4	•	•	•	•	•					
D8 $-$ $\overline{\text{D8}}$	•	•	•	•		•	•	•	•	•

The chiral symmetry in QCD is therefore realized as the gauge symmetry of the D8 $-$ $\overline{\text{D8}}$ pairs. The radial coordinate U transverse to the D4-branes is bounded from below, due to an existing horizon in the supergravity background for $U \geq U_{KK}$. In the limit of $U \to U_{KK}$

the radius of the S^1 shrinks to zero. At some point[1] $U = U_0$, the D8 brane-pairs merge into a single component, resulting in the reduction to just one $U(N_f)$ gauge symmetry. Thus, this brane configuration yields an intuitive picture for holographically breaking the chiral symmetry.

Although it is to be expected that this model is in the same universality class as the four-dimensional massless large N_c QCD, those theories are not equivalent in the high energy regime. As is generally the case when compactifying branes to a circle, an infinite tower of Kaluza-Klein modes of mass scale M_{KK} arises. These modes are not observed in QCD and therefore have to be much heavier than the states which appear in QCD. Also, since our brane configuration is invariant under rotations of the $x^{5\ldots9}$ plane, there also exists an $SO\,(5)$ symmetry. Therefore, only singlet states with respect to this symmetry are used, as QCD does not have such a symmetry.

5.1 Properties of the Brane System

The compactified direction of this brane system is x^4 with a radius of M_{KK}^{-1}. M_{KK} is the Kaluza-Klein mass defining the energy scale of this brane system, i.e. at energies lower than M_{KK} we obtain a four-dimensional $U(N_c)$ gauge theory in the D4-brane world volume. Therefore for the different types of strings we have:

- 4−4 strings are open strings with both ends attached to the D4-brane, representing fermions in the adjoint representation of $U\,(N_c)$ and gauge field bosons. By the imposition of the boundary conditions, the former acquire masses of order M_{KK}. The massless modes of those strings are:
  - the gauge field $A_\mu^{(\mathrm{D4})}$ with $(\mu = 0, 1, 2, 3)$
  - the scalar fields $A_4^{(\mathrm{D4})}$ and Φ^i with $(i = 5, 6, 7, 8, 9)$
- 4−8 strings are open strings attached on one end to the D4 brane and on the other to D8. At high energies, they represent N_f flavors of massless fermions in the fundamental representation of $U(N_c)$ and are interpreted as quarks. The 4−$\overline{8}$ strings, on the other hand, then have opposite chirality. The low-energy modes correspond to mesons and are represented as:
  - $A_\mu^{(\mathrm{D8})}$
  - $A_z^{(\mathrm{D8})}$, see section 5.3
- 8−$\overline{8}$ strings create a tachyon field that becomes massive by separating the D8 − $\overline{\mathrm{D8}}$ pair along the x^4 direction, which is essential for the chiral interpretation of the geometry. The mass of the tachyon mode is then given as

$$m^2 = \left(\frac{\Delta x^4}{2\pi\alpha'}\right)^2 - \frac{1}{2\alpha'} \tag{5.1.1}$$

[1] In the original WSS model one has $U_0 = U_{KK}$, which corresponds to an antipodal embedding of the flavour branes

and for $\Delta x^4 \gg \sqrt{\alpha'}$, the tachyon becomes massive and can be neglected in the massless spectrum. Since no $8-\overline{8}$ strings are involved, the massless spectrum on the D4-brane and the minimal couplings among them are not affected by the separation Δx^4.

5.2 D4 Background

The $\mathrm{D8}-\overline{\mathrm{D8}}$ brane system is then described in terms of supergravity. The solution for the D4-brane reads

$$\mathrm{d}s^2 = \left(\frac{U}{R}\right)^{\frac{3}{2}} \left(\eta_{\mu\nu} dx^\mu dx^\nu + f\left(U\right) d\tau^2\right) + \left(\frac{R}{U}\right)^{\frac{3}{2}} \left(\frac{dU^2}{f\left(U\right)} + U^2 d\Omega_4^2\right) \tag{5.2.1}$$

with

$$e^\phi = g_s \left(\frac{U}{R}\right)^{\frac{3}{4}}, \quad F_4 = dC_3 = \frac{2\pi N_c}{V_4}\epsilon_4, \quad f(U) = 1 - \frac{U_{KK}^3}{U^3} \tag{5.2.2}$$

where $d\Omega_4^2$, ϵ_4 and $V_4 = \frac{8\pi^2}{3}$ are the line element, volume form and volume of a unit S_4, respectively and e^ϕ is the dilaton. The D4-branes are extended in the x^μ ($\mu = 0, 1, 2, 3$) and τ directions. R is the AdS radius of the D4 background and related to the string coupling and string length via

$$R^3 = \pi g_s N_c l_s^3 \,. \tag{5.2.3}$$

The coordinate U is bounded from below via $U \geq U_{KK}$ and in order to avoid a singularity at $U = U_{KK}$, τ must be periodic with

$$\tau \sim \tau + \delta\tau \,, \quad \delta\tau \equiv \frac{4\pi}{3}\frac{R^{3/2}}{U_{KK}^{1/2}} \,. \tag{5.2.4}$$

The Kaluza-Klein mass is defined as

$$M_{KK} = \frac{2\pi}{\delta\tau} = \frac{3}{2}\frac{U_{KK}^{1/2}}{R^{3/2}} \tag{5.2.5}$$

and specifies the energy scale below which the dual theory reduces to four-dimensional Yang-Mills theory. The Yang-Mills coupling at the cutoff scale M_{KK} is related to the string coupling via

$$g_{YM}^2 = \frac{(2\pi)^2 g_s l_s}{\delta\tau} \tag{5.2.6}$$

The supergravity description relates the parameters R, U_{KK} and g_s

$$R^3 = \frac{1}{2}\frac{g_{YM}^2 N_c l_s^2}{M_{KK}}, \quad U_{KK} = \frac{2}{9} g_{YM}^2 N_c M_{KK} l_s^2, \quad g_s = \frac{1}{2\pi}\frac{g_{YM}^2}{M_{KK} l_s}. \tag{5.2.7}$$

In order to show the stability of the embedding of the D8-brane into the D4 background, the induced metric on the D8-brane has to be introduced and the resulting equation of motion needs to be checked. This procedure shows that the probe configuration is stable with respect to small fluctuations, cf. [38].

5.3 Gauge Field on the D8-brane

Going back to the initial definition of the geometry of this model, it is clear that the gauge field on the D8-brane has nine components:

- A_μ with $\mu = 0, 1, 2, 3$
- A_z
- $A_\alpha = 0$ where $\alpha = 5, 6, 7, 8$ are the coordinates on the S^4.

All the α components are set to zero, since we are only considering $SO(5)$ singlet states. With these considerations, we can define the action of the brane via the so-called *DBI action*. It is a general result for the action on branes and can be defined and used for all different dimensionalities of the branes concerned. Essentially it is just a generalisation of the Nambu-Goto action for higher dimensions and gauge fields living on the brane. Therefore, it only depends on the induced metric, also called pullback, on the brane with respect to the background, the gauge fields and the dilaton. In general terms it reads for a D8-brane in the mostly plus convention:

$$S_{\mathrm{D8}} = -T_8 \int \mathrm{d}^9x\, e^{-\phi} \sqrt{-\det(g_{MN} + 2\pi\alpha' F_{MN})} + S_{CS}, \tag{5.3.1}$$

where $T_8 = (2\pi)^{-8} l_s^{-9}$ is the tension of the brane, g_{MN} is the induced metric and F_{MN} the field strength tensor. S_{CS} is the Chern-Simons contribution to the action, given by

$$S_{CS} = \mu \int_{\mathrm{D8}} C_3 \operatorname{Tr} F^3 \tag{5.3.2}$$

$$= \mu \int_{\mathrm{D8}} F_4 \omega_5(A), \tag{5.3.3}$$

with the normalization constant $\mu = 1/48\pi^3$ and the RR 4-form field strength $F_4 = dC_3$ and the Chern-Simons 5-form

$$\omega_5(A) = \operatorname{Tr}\left(AF^2 - \frac{1}{2}A^3F + \frac{1}{10}A^5\right), \tag{5.3.4}$$

satisfying $\mathrm{d}\omega_5 = \operatorname{Tr} F^3$. The Chern-Simons term is crucial for studying the chiral anomaly [37], but will be omitted in the following, since for our study this term is not of any interest. Using the assumptions on the gauge fields and plugging everything into (5.3.1), one gets

$$S_{\mathrm{D8}} = -\tilde{T}\left(2\pi\alpha'\right)^2 \int \mathrm{d}^4x\, \mathrm{d}z \left[\frac{R^3}{4U_z}\eta^{\mu\nu}\eta^{\rho\sigma}F_{\mu\rho}F_{\nu\sigma} + \frac{9}{8}\frac{U_z^3}{U_{KK}}\eta^{\mu\nu}F_{\mu z}F_{\nu z}\right] + \mathcal{O}\left(F^3\right), \tag{5.3.5}$$

where $U_z \equiv \left(U_{KK}^3 + z^2 U_{KK}\right)^{\frac{1}{3}}$ and $\tilde{T} = \frac{2}{3}R^{\frac{3}{2}}U_{KK}^{\frac{1}{2}}T_8 V_4 g_s^{-1}$. In order to define the field strengths, the gauge fields are expanded in terms of complete sets $\{\psi_n(z)\}_{n\geq 1}$ and $\{\varphi_n(z)\}_{n\geq 0}$:

$$A_\mu(x^\mu, z) = \sum_n B_\mu^{(n)}(x^\mu)\psi_n(z), \tag{5.3.6}$$

$$A_z(x^\mu, z) = \varphi^{(0)}(x^\mu)\phi_0(z) + \sum_{n=1} \varphi^{(n)}(x^\mu)\phi_n(z), \tag{5.3.7}$$

where $B_\mu^{(n)}$ are the vector meson fields and $\varphi^{(n)}$ are scalar fields. In terms of those fields, the field strengths of (5.3.5) are then given by

$$F_{\mu\nu}(x^\mu, z) = \sum_n \Big(\partial_\mu B_\nu^{(n)}(x^\mu) - \partial_\nu B_\mu^{(n)}(x^\mu)\Big)\psi_n(z) \tag{5.3.8}$$

$$\equiv \sum_n F_{\mu\nu}^{(n)}(x^\mu)\psi_n(z), \tag{5.3.9}$$

$$F_{\mu z}(x^\mu, z) = \sum_n \Big(\partial_\mu \varphi^{(n)}(x^\mu)\phi_n(z) - B_\mu^{(n)}(x^\mu)\dot{\psi}_n(z)\Big). \tag{5.3.10}$$

Dropping the terms with $\phi^{(n)}$, the action is then rewritten as

$$S_{\text{D8}} = -\tilde{T}\big(2\pi\alpha'\big)^2 R^3 \int \mathrm{d}^4x\, \mathrm{d}Z \sum_{m,n}\Big[\frac{1}{4}K^{-\frac{1}{3}}F_{\mu\nu}^{(m)}F^{\mu\nu(m)}\psi_n\psi_m + \frac{1}{2}M_{KK}^2 K B_\mu^{(m)}B^{\mu(m)}\partial_Z\psi_m\partial_Z\psi_n\Big], \tag{5.3.11}$$

where the dimensionless coordinate Z is defined by

$$Z \equiv \frac{z}{U_{KK}}, \qquad K(Z) = 1 + Z^2 = \left(\frac{U_z}{U_{KK}}\right)^3. \tag{5.3.12}$$

The functions ψ_n must satisfy the eigenvalue equation

$$-K^{\frac{1}{3}}\partial_Z(K\partial_Z\psi_n) = \lambda_n\psi_n \tag{5.3.13}$$

with the normalization condition

$$\tilde{T}\big(2\pi\alpha'\big)^2 R^3 \int \mathrm{d}Z\, K^{-\frac{1}{3}}\psi_n\psi_m = \delta_{nm}. \tag{5.3.14}$$

This leads to

$$\tilde{T}\big(2\pi\alpha'\big)^2 R^3 \int \mathrm{d}Z\, K\partial_Z\psi_m\partial_Z\psi_n = \lambda_n\delta_{nm} \tag{5.3.15}$$

and

$$S_{\text{D8}} = \int \mathrm{d}^4x \sum_{n=1}\left[F_{\mu\nu}^{(n)}F^{\mu\nu(n)} + \frac{1}{2}m_n^2 B_\mu^{(n)}B^{\mu(n)}\right], \tag{5.3.16}$$

where the mass of the vector mesons is given by $m_n^2 \equiv \lambda_n M_{KK}^2 > 1$. On the other hand, the functions $\phi_n(z)$ are chosen to satisfy $\phi_n(Z) \propto \partial_Z\psi_n(Z)$ and the pseudoscalar-mode, representing the Goldstone bosons of chiral symmetry breaking, is defined as

$$\phi_0 = \frac{1}{\sqrt{\pi\kappa}K(z)M_{KK}}, \tag{5.3.17}$$

with

$$\kappa = \frac{\lambda N_c}{216\pi^3}, \tag{5.3.18}$$

where λ is the 't Hooft coupling. The null-mode satisfies the orthonormal condition

$$(\phi_m, \phi_n) \equiv \frac{9}{4}\tilde{T}\big(2\pi\alpha'\big)^2 U_{KK}^3 \int \mathrm{d}Z\, K\phi_n\phi_m = \delta_{nm}. \tag{5.3.19}$$

The field strength (5.3.10) can then be rewritten as

$$F_{\mu z} = \partial_\mu \phi^{(0)} + \sum_{n\geq 1} \left(m_n^{-1} \partial_\mu \phi^{(n)} - B_\mu^{(n)} \right) \dot{\psi}_n \tag{5.3.20}$$

and by absorbing the first term in the parenthesis via the gauge transformation

$$B_\mu^{(n)} \to B_\mu^{(n)} + m_n^{-1} \partial_\mu \phi^{(n)}, \tag{5.3.21}$$

the action (5.3.5) can be rewritten as

$$S_{\mathrm{D8}} = -\int \mathrm{d}^4 x \left[\frac{1}{2} \left(\partial_\mu \varphi^{(0)} \right)^2 + \sum_{n\geq 1} \left(\frac{1}{4} F_{\mu\nu}^{(n)} F^{\mu\nu(n)} + \frac{1}{2} m_n^2 B_\mu^{(n)} B^{\mu(n)} \right) \right], \tag{5.3.22}$$

where $\varphi^{(0)}$ is the massless pion field and $B_\mu^{(n)}$ represents a tower of vector fields of mass squared λ_n which are interpreted as vector mesons.

Going back to the $U(N_f)_L \times U(N_f)_R$ chiral symmetry, we now take a look at the interaction of the mesons with the external gauge fields $A_{L\mu}$ and $A_{R\mu}$. Since photons couple in the same way to the left and right parts, the couplings of the mesons to the photon field can be found via

$$A_{L\mu} = A_{R\mu} = e \mathcal{Q} A_\mu^{em}, \tag{5.3.23}$$

where e is the electromagnetic coupling constant and $\mathcal{Q}$ is the electric charge matrix, in our case given by

$$\mathcal{Q} = \frac{1}{3} \begin{pmatrix} 2 & & \\ & -1 & \\ & & -1 \end{pmatrix}, \tag{5.3.24}$$

where in principle more quark flavors could be considered as well, but so far we will stick to this definition of $\mathcal{Q}$ in the case of $N_f = 3$. In the next step the external gauge fields are introduced by imposing the asymptotic values of the A_μ field on the D8-brane as

$$\lim_{z\to+\infty} A_\mu(x^\mu, z) = A_{L\mu}(x^\mu) \quad \text{and} \quad \lim_{z\to-\infty} A_\mu(x^\mu, z) = A_{R\mu}(x^\mu), \tag{5.3.25}$$

reflecting the fact that the D8-branes of different chirality lie on antipodal points of the background geometry. One therefore gets a modified mode expansion (5.3.6):

$$A_\mu(x^\mu, z) = A_{L\mu}(x^\mu)\psi_+(z) + A_{R\mu}(x^\mu)\psi_-(z) + \sum_{n=1}^{\infty} B_\mu^{(n)} \psi_n(z), \tag{5.3.26}$$

with

$$\psi_\pm(z) \equiv \frac{1}{2}(1 \pm \psi_0(z)), \quad \psi_0(z) \equiv \frac{2}{\pi} \arctan z, \quad \partial_z \psi_\pm(z) \propto \phi_0(z), \tag{5.3.27}$$

where $\psi_\pm(z)$ are the non-renormalizable zero modes of (5.3.13).

Using this expansion of A_μ in the integration of action (5.3.5) yields divergent coefficients of the kinetic terms of the left and right gauge fields. This reflects the vanishing gauge

coupling corresponding to the $U(N_f)_L \times U(N_f)_R$ symmetry. Although this divergences could be circumvented by a suitable cut-off, in the following we will simply ignore those divergent terms as they are of no interest in the study conducted here.

In the following we make a distinction between vector and axial-vector fields, using the notation

$$\mathcal{V}_\mu \equiv \frac{1}{2}(A_{L\mu} + A_{R\mu}), \quad \mathcal{A}_\mu \equiv \frac{1}{2}(A_{L\mu} - A_{R\mu}), \quad v_\mu^n \equiv B_\mu^{(2n-1)}, \quad a_\mu^n \equiv B_\mu^{(2n)}, \tag{5.3.28}$$

where $\mathcal{V}$ is the photon field.

Rewriting the gauge field (5.3.6) in terms of these fields yields

$$A_\mu(x^\mu, z) = \mathcal{V}_\mu(x^\mu) + \mathcal{A}_\mu(x^\mu)\psi_0(z) + \sum_{n=1}^{\infty} v_\mu^n(x^\mu)\psi_{2n-1}(z) + \sum_{n=1}^{\infty} a_\mu^n(x^\mu)\psi_{2n}(z), \tag{5.3.29}$$

where in the following we will drop the terms with axial fields $\mathcal{A}_\mu$ and a_μ, as they do not contribute to the discussion conducted here. With this definition and also using the completeness relation

$$\kappa \sum_n K^{-\frac{1}{3}}(z')\psi_n(z)\psi_n(z') = \delta(z - z'), \tag{5.3.30}$$

we can rewrite the first term of the action (5.3.5) as

$$\begin{aligned} S_{\mathrm{D8}}^{(1)} &= \kappa \int \mathrm{d}^4x\, \mathrm{d}z\, \mathrm{Tr}\left[\frac{1}{2}K^{-\frac{1}{3}}(z)F_{\mu\nu}^2(x^\mu, z)\right] \\ &\supseteq \frac{\kappa}{2}\int \mathrm{d}^4x\, \mathrm{Tr}\Big[a_{\mathcal{V}\mathcal{V}}\big(\partial_\mu\mathcal{V}_\nu - \partial_\nu\mathcal{V}_\mu\big)^2 + \big(\partial_\mu v_\nu^n - \partial_\nu v_\mu^n\big)^2 \\ &\qquad + a_{\mathcal{V}v^n}\big(\partial_\mu\mathcal{V}_\nu - \partial_\nu\mathcal{V}_\mu\big)\big(\partial_\mu v_\nu^n - \partial_\nu v_\mu^n\big)\Big] \end{aligned} \tag{5.3.31}$$

where the couplings are given by

$$a_{\mathcal{V}\mathcal{V}} = \kappa \int \mathrm{d}z\, K^{-\frac{1}{3}}, \qquad a_{\mathcal{V}v^n} = \kappa \int \mathrm{d}z\, K^{-\frac{1}{3}}\psi_{2n-1}. \tag{5.3.32}$$

Since (5.3.31) mixes the photon field with the vector fields, the Sakai-Sugimoto model reproduces vector meson dominance (VMD).

Chapter 6

Glueballs and their Couplings

In this chapter, we discuss the glueball spectrum as derived from metric fluctuations in the stringy background. Inserting these fluctuations into the background, provided by the Sakai-Sugimoto model, yields the effective interaction Lagrangian for glueballs and vector mesons. However, since these calculations are rather involved, we will only sketch the derivations and only present the key formulas and results. For further information, please refer to [41–46]. The coupling of the Pomeron to the proton, as well as the Pomeron propagator are then found by means of comparing results from Regge theory and String theory. The exchange of a trajectory of glueball states, which we identify as the Pomeron, corresponds to closed string scattering, justifying the procedure. For the full discussion we refer to [15, 47–49] and references therein.

6.1 Metric Fluctuations

Gravitons arise as spin-two excitations for the effective p-dimensional theory. Those excitations are associated with the stress-energy tensor $T_{\mu\nu}$ of the conformal field theory as this is the dual to the AdS-metric perturbations which are identified with gravitons. In general the AdS soliton metric is written as

$$\mathrm{d}s^2 = \frac{r^2}{L^2}\left(f(r)\,\mathrm{d}\tau^2 + \eta_{\mu\nu}\,\mathrm{d}x^\mu\,\mathrm{d}x^\nu\right) + \frac{L^2}{r^2}f^{-1}(r)\,\mathrm{d}r^2\,, \tag{6.1.1}$$

with

$$f(r) = \left(1 - \frac{R^{p+1}}{r^{p+1}}\right). \tag{6.1.2}$$

This geometry is only locally asymptotically AdS though, since in order to avoid a conical singularity at $r = R$ the coordinate τ is chosen to be periodic $\tau = \tau + 2\pi\beta$ with

$$\beta = \frac{4\pi L^2}{(p+1)R}. \tag{6.1.3}$$

Imposing anti-periodic boundary conditions for fermions on this circle, i.e. fermions pick up a minus sign when moving around the circle, also breaks supersymmetry without the

explicit inclusion of additional Supersymmetry (SUSY)-breaking terms in the action. In order to find the spectrum of gravitons on the background (6.1.1) one solves the equations of motion and writes the perturbed metric as

$$g_{ab} = \bar{g}_{ab} + h_{ab}, \tag{6.1.4}$$

where h_{ab} describes the fluctuations of the background metric $\bar{g}_{ab}$. Linearizing the equations of motion of the Einstein equation, see e.g. [50],

$$R_{ab} + \frac{p+1}{L^2} g_{ab} = 0 \tag{6.1.5}$$

leads (i.e. in the transverse traceless gauge, for easier computation) to the condition for h_{ab}

$$\frac{1}{2}\nabla_a \nabla_b h^c{}_c + \frac{1}{2}\nabla^2 h_{ab} - \nabla^c \nabla_{(a} h_{b)c} - \frac{p+1}{L^2} h_{ab} = 0, \tag{6.1.6}$$

where in the following the ansatz for the gravitons

$$h_{ab} = H_{ab}(r) e^{ik\cdot x} \tag{6.1.7}$$

is used, where $H_{ab}(r)$ is the radial profile of the tensor and k^μ is a p-dimensional momentum vector with $k^2 = -M^2$. One can further define

$$H_{ab} = \varepsilon_{ab} \frac{r^2}{L^2} H(r), \tag{6.1.8}$$

where ε_{ab} is a constant traceless polarization tensor.

Given this preliminaries, we will now take a look at what solutions one gets for the IIA stringy background.

6.2 Stringy Background

In the model presented in [51] one works in terms of type IIA string theory and arrives at a dual of QCD_4, but in order to find the graviton modes corresponding to the glueball states of interest, i.e. the tensor 2^{++} state, we will start with the overall geometrical construction of 11 dimensional M-theory (Sugra) on $\mathrm{AdS}_7 \times \mathrm{S}_4$. The AdS part has Euclidean space-time coordinates x_1, x_2, x_3, x_4, x_5 and x_{11} as well as a radial coordinate r. Coordinates on S^4 are denoted by x_α with $\alpha = 7, 8, 9, 10$. Now one compactifies x_{11} like it is presented in appendix B.1 resulting in type IIA string theory. The D4 background considered in the model of Sakai and Sugimoto yields a five-dimensional Yang-Mills CFT, which upon compactifying $x_5 = \tau$ on a pseudo thermal circle, where $\beta = \frac{2\pi}{M_{KK}}$, is dimensionally reduced to QCD_4.

In order to find the glueball modes of interest one is only interested in excitations which are compatible with QCD_4 and therefore all Kaluza-Klein modes arising from compactification are ignored and only SO(5) singlet states are considered. These restrictions reduce the problem to six independent wave equations from which we are only interested in T_4.

6.3 Glueball Spectrum

In the strong coupling limit at large N, where string theory becomes classical gravity in the AdS_7 black hole metric defined as

$$ds^2 = \left(r^2 - \frac{1}{r^4}\right) d\tau^2 + r^2 \sum_{i=1,2,3,4,11} dx_i{}^2 + \left(r^2 - \frac{1}{r^4}\right)^{-1} dr^2 + \frac{1}{4} d\Omega_4{}^2 , \tag{6.3.1}$$

where the radius of curvature R_{AdS} is related to the radius of the S_4 L via

$$R_{\text{AdS}} = \frac{L}{2}. \tag{6.3.2}$$

In generic M-theory the supergraviton spectrum consists of the graviton G_{MN} and a 3-form field A_{MNL}, where in our case we are only considering the former. After the procedure presented above, one is therefore left with a graviton $G_{\mu\nu}$, a dilaton ϕ and a NS-NS tensor field $B_{\mu\nu}$, with $\mu, \nu = \{1, \ldots, 10\}$. We are only interested in the $J^{PC} = 2^{++}$ state, which is given by G_{ij} and the quadratic fluctuations in the AdS_7 background that survive for QCD_4 in the weak coupling limit. In order to count the number of independent fluctuations for a field of given spin one considers harmonic plane waves propagating in the AdS radial direction, r, with euclidean time, x_4, without any dependence on the spatial coordinates x_1, x_2, x_3, x_{11} and the compactified direction τ.

As established in (6.1.8), gravitons have two polarization indices. Since the polarization tensor has to be traceless, one is left with $\frac{5\times 6}{2} - 1 = 14$ independent components. In the case of a flat background this holds generally, but for AdS this form of polarization only will occur for $r \to \infty$.

The background metric is flat in the first four directions, i.e. $g_{11} = g_{22} = g_{33} = g_{11,11} = r^2$ and warped in the τ direction, with $g_{\tau\tau} = r^2 - r^{-4}$. In other words, the system has $SO(4)$ symmetry which breaks up into $9, 4$ and 1 dimensional irreducible representations under $SO(4)$ leading to three distinct equations, where we are only interested in the one denoted by T_4. The 9-dimensional representation leads to a degenerate spectrum of spins under the physical $SO(3)$ symmetry and breaks into $5 \oplus 3 \oplus 1$, yielding for the 2^{++}-state G_{ij}:

$$h_{ij} - \frac{1}{3}\delta_{ij} h_{kk} \neq 0, \tag{6.3.3}$$

with $i, j, k = 1, 2, 3$. A full list of metric perturbations can be found in [43]. Analyzing the linearized Einstein equations (6.1.6) for the AdS background presented above then leads to the three independent equations mentioned earlier, T_4, V_4 and S_4, where the equation for T_4 is given as

$$\frac{d}{dr}\left(r^7 - r\right)\frac{d}{dr} T_4(x) + \left(m^2 r^3\right) T_4(r) = 0 \tag{6.3.4}$$

Considering the following metric perturbations (cf. (6.1.7))

$$h_{\mu\nu} = \epsilon_{\mu\nu}(r) e^{ik_4 x_4}, \tag{6.3.5}$$

with $k_4 = im$ and fixing the gauge to $h_{4\mu} = 0$, the tensor h_{ij} of (6.3.3) can be written as

$$h_{ij} = q_{ij} r^2 T_4(r) e^{-m x_4}, \tag{6.3.6}$$

where q_{ij} is an arbitrary constant traceless and symmetric 3×3 matrix.

6.4 Interactions with Mesons

The effective interaction Lagrangian for glueballs and mesons in the Sakai Sugimoto model are then found by inserting the respective metric fluctuation in the D8 brane action and then integrating over the bulk coordinates. Following [46], the interactions for the tensor glueball are described via

$$\mathcal{L}_{\mathcal{G}vv} = \frac{1}{2}\mathrm{Tr}\Big[t_2 M_{KK}^2 v_\mu v_\nu \mathcal{G}^{\mu\nu} + t_3 F_{\mu\rho} F_\nu{}^\rho \mathcal{G}^{\mu\nu}\Big], \tag{6.4.1}$$

where there also exist many other interactions with baryons, pseudoscalar-, vector- and axial vector-fields, hence the indexing. The couplings t_2 and t_3 are again given by the expressions

$$t_2^{mn} = \kappa \int \mathrm{d}z\, K \psi'_{2m-1}(z) \psi'_{2n-1}(z) T_4(z), \tag{6.4.2}$$

$$t_3^{mn} = \kappa \int \mathrm{d}z\, K^{-\frac{1}{3}} \psi_{2m-1}(z) \psi_{2n-1}(z) T_4(z), \tag{6.4.3}$$

where $T_4(z)$ is the radial profile of the glueball, see (6.3.4). Replacing the vector mesons with photons by using VMD twice in (6.4.1) yields

$$\begin{aligned}\mathcal{L}_{\mathcal{G}\mathcal{V}\mathcal{V}} = \mathrm{Tr}\Big[& t_2^{\mathcal{V}^*\mathcal{V}^*}(Q_1, Q_2) \frac{Q_1^2 Q_2^2}{M_{KK}^2} \mathcal{V}_\mu \mathcal{V}_\nu \mathcal{G}^{\mu\nu} \\ & + t_3^{\mathcal{V}^*\mathcal{V}^*}(Q_1, Q_2) \mathcal{G}^{\mu\nu}\, \mathrm{Tr}\Big(F_{\mu\rho}^{\mathcal{V}^*\mathcal{V}^*} F_\nu{}^{\rho\mathcal{V}^*}\Big)\Big],\end{aligned} \tag{6.4.4}$$

with

$$t_2^{\mathcal{V}^*\mathcal{V}^*}(Q_1, Q_2) = \frac{M_{KK}^4}{Q_1^2 Q_2^2} \kappa \int \mathrm{d}z\, K \mathcal{J}'(Q_1, z) \mathcal{J}'(Q_2, z) T_4(z), \tag{6.4.5}$$

$$t_3^{\mathcal{V}^*\mathcal{V}^*}(Q_1, Q_2) = \kappa \int \mathrm{d}z\, K^{-\frac{1}{3}} \mathcal{J}(Q_1, z) \mathcal{J}(Q_2, z) T_4(z), \tag{6.4.6}$$

where the off-shell bulk-to-boundary propagator $\mathcal{J}$, cf. (5.3.13), was introduced with

$$\big(1 + z^2\big)^{\frac{1}{3}} \partial_z \big[\big(1 + z^2\big) \partial_z \mathcal{J}\big] = \frac{Q^2}{M_{KK}^2} \mathcal{J} \tag{6.4.7}$$

6.5 Glueball Coupling to Photons

We will now use the interaction Lagrangian (6.4.4) in order to determine the vertex factors for the glueball-photon-photon vertex. We will do this by means of functional derivation. The diagram for the process is shown in figure 6.1.

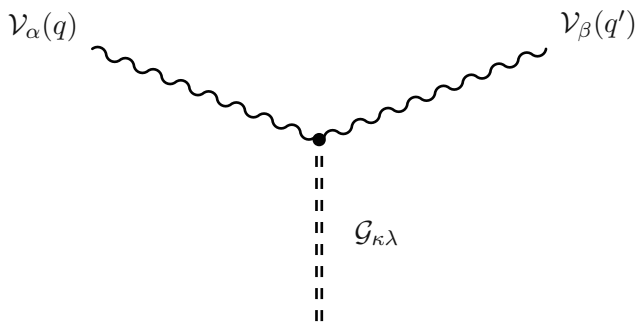

Figure 6.1. Feynman diagram for (6.4.4).

Dropping the prefactors and the couplings we calculate the vertex factor of the first term in the interaction Lagrangian $\mathcal{L}_1$ as

$$\begin{aligned}\frac{1}{i^3}\frac{\delta\mathcal{L}_1}{\delta\mathcal{V}_\alpha\mathcal{V}_\beta\mathcal{G}_{\kappa\lambda}} &= i\eta^{\mu\kappa}\eta^{\nu\lambda}\frac{\delta}{\delta\mathcal{V}_\alpha\mathcal{V}_\beta}\mathcal{V}_\mu\mathcal{V}_\nu = i\eta^{\mu\kappa}\eta^{\nu\lambda}\Big(\delta^\alpha_\mu\delta^\beta_\nu+\delta^\alpha_\nu\delta^\beta_\mu\Big)\\ &= i\Big(\eta^{\alpha\kappa}\eta^{\beta\lambda}+\eta^{\beta\kappa}\eta^{\alpha\lambda}\Big)\end{aligned} \tag{6.5.1}$$

The second term $\mathcal{L}_2$ is not as straightforward as one has to express the field strengths in terms of the photon field $\mathcal{V}_\mu$. Here we also ignore the prefactors, couplings and the trace for now and get

$$\frac{1}{i^3}\frac{\delta\mathcal{L}_2}{\delta\mathcal{V}_\alpha\mathcal{V}_\beta\mathcal{G}_{\kappa\lambda}} = i\eta^{\mu\kappa}\eta^{\nu\lambda}\frac{\delta}{\delta\mathcal{V}_\alpha\mathcal{V}_\beta}\Big[(\partial_\mu\mathcal{V}_\rho-\partial_\rho\mathcal{V}_\mu)(\partial_\nu\mathcal{V}^\rho-\partial^\rho\mathcal{V}_\nu)\Big] \tag{6.5.2}$$

with

- $\partial_\mu\mathcal{V}_\rho\partial_\nu\mathcal{V}^\rho \longrightarrow i^2 2\eta^{\alpha\beta}q_\mu q'_\nu$
- $-\partial_\mu\mathcal{V}_\rho\partial^\rho\mathcal{V}_\nu \longrightarrow -i^2 q_\mu q'^\rho\Big(\delta^\alpha_\rho\delta^\beta_\nu+\delta^\alpha_\nu\delta^\beta_\kappa\Big)$
- $-\partial_\rho\mathcal{V}_\mu\partial_\nu\mathcal{V}^\rho \longrightarrow -i^2 q_\rho q'_\nu\Big(\delta^\alpha_\mu\eta^{\beta\rho}+\delta^\beta_\mu\eta^{\alpha\rho}\Big)$
- $\partial_\rho\mathcal{V}_\mu\partial^\rho\mathcal{V}_\nu \longrightarrow i^2 q_\rho q'^\rho\Big(\delta^\alpha_\mu\delta^\beta_\nu+\delta^\alpha_\nu\delta^\beta_\mu\Big)$.

Since in forward scattering we have $q=-q'$ we get

$$\begin{aligned}\frac{\delta\mathcal{L}_2}{\delta\mathcal{V}_\alpha\mathcal{V}_\beta\mathcal{G}_{\kappa\lambda}} &= -i\eta^{\mu\kappa}\eta^{\nu\lambda}\Big[q_\mu q^\rho\Big(\delta^\alpha_\rho\delta^\beta_\nu+\delta^\alpha_\nu\delta^\beta_\rho\Big)+q_\rho q_\nu\Big(\delta^\alpha_\mu\eta^{\beta\rho}+\delta^\beta_\mu\eta^{\alpha\rho}\Big)\\ &\qquad -2\eta^{\alpha\beta}q_\mu q_\nu - q^2\Big(\delta^\alpha_\mu\delta^\beta_\nu+\delta^\alpha_\nu\delta^\beta_\mu\Big)\Big]\\ &= -i\Big(\eta^{\beta\lambda}q^\kappa q^\alpha+\eta^{\alpha\lambda}q^\kappa q^\beta+\eta^{\alpha\kappa}q^\beta q^\lambda+\eta^{\beta\kappa}q^\alpha q^\lambda\\ &\qquad -2\eta^{\alpha\beta}q^\kappa q^\lambda - q^2\Big(\eta^{\alpha\kappa}\eta^{\beta\lambda}+\eta^{\beta\kappa}\eta^{\alpha\lambda}\Big)\Big)\end{aligned} \tag{6.5.3}$$

Restoring the dropped prefactors and also the ones we have from VMD, see (5.3.23), as well as the trace we get as a final result for the vertex

$$\begin{aligned}\mathbb{V}^{\alpha\beta\kappa\lambda}_{\mathcal{G}\mathcal{V}\mathcal{V}} = ie^2\,\mathrm{Tr}\big(\mathcal{Q}^2\big)\Bigg[&\frac{t_2 q^4}{M_{KK}^2}\Big(\eta^{\alpha\kappa}\eta^{\beta\lambda}+\eta^{\beta\kappa}\eta^{\alpha\lambda}\Big)\\ &- t_3\Big(\eta^{\beta\lambda}q^\kappa q^\alpha+\eta^{\alpha\lambda}q^\kappa q^\beta+\eta^{\alpha\kappa}q^\beta q^\lambda+\eta^{\beta\kappa}q^\alpha q^\lambda\\ &- 2\eta^{\alpha\beta}q^\kappa q^\lambda - q^2\Big(\eta^{\alpha\kappa}\eta^{\beta\lambda}+\eta^{\beta\kappa}\eta^{\alpha\lambda}\Big)\Big)\Bigg]\end{aligned} \tag{6.5.4}$$

6.6 Glueball-Proton Coupling and Pomeron Propagator

Since there is no known way of calculating the full tree-level string amplitudes in curved backgrounds, certain approximations need to be put into place:

- Approximate the scattering amplitude with the Virasoro-Shapiro amplitude for the scattering of four closed string tachyons in flat space.
- Calculate the coupling of the Pomeron to the proton as the vertex of a proton and a 2^{++}-glueball (i.e. the lowest state on the Pomeron trajectory).
- Convert this amplitude into the Regge limit of a full tree-level string amplitude via "Reggeization".

6.6.1 Proton Coupling

As already stated in (6.3.3), the glueball field can be treated as a rank-2 symmetric traceless tensor $h_{\mu\nu}$ and should therefore couple predominantly to the QCD stress-energy tensor $T^{\mu\nu}$ in the following way [15]

$$S_{\text{int}} = \lambda_{\mathcal{P}} \int \mathrm{d}^4x\, h_{\mu\nu}T^{\mu\nu}. \tag{6.6.1}$$

Under this assumption the glueball-proton-proton vertex is given by

$$\Gamma^{\mathcal{G}pp}_{\mu\nu} = \big\langle p', s'\big|T_{\mu\nu}(0)\big|p, s\big\rangle\,. \tag{6.6.2}$$

This matrix element can be written in terms of form factors, using the symmetry and conservation of $T_{\mu\nu}$, as

$$\begin{aligned}\Gamma^{\mathcal{G}pp}_{\mu\nu} = \lambda_{\mathcal{P}}\bar{u}\big(p', s'\big)\Bigg[&A(t)\frac{\gamma_\mu P_\nu+\gamma_\nu P_\mu}{2}+B(t)\frac{i(P_\mu\sigma_{\nu\rho}+P_\nu\sigma_{\mu\rho})k^\rho}{4m_p}\\ &+C(t)\frac{\big(k_\mu k_\nu-\eta_{\mu\nu}k^2\big)}{m_p}\Bigg]u(p,s),\end{aligned} \tag{6.6.3}$$

where $k = p - p'$, $t = k^2$ and $P = \frac{p+p'}{2}$. This general form of the matrix element reduces to only the first term, as for the proton with spin $\frac{1}{2}$ and mass m_p the coefficients are implied

to be constrained to $A(0) = 1$, $B(0) = 0$ and the contribution from $C(t)$ is suppressed in the Regge limit. We therefore simply get for the vertex

$$\Gamma^{\mathcal{G}pp}_{\mu\nu} = \lambda_{\mathcal{P}} \left[\bar{u}(p', s') \frac{\gamma_\mu P_\nu + \gamma_\nu P_\mu}{2} u(p, s) \right]. \tag{6.6.4}$$

We can now further simplify this expression by calculating the sums over the spins of the initial- and final-state spinor via the completeness relation

$$\sum_{s=1,2} u_s \bar{u}_s = \gamma_\alpha p^\alpha + m. \tag{6.6.5}$$

Using Casimir's trick, c.f. [52], we rewrite expression (6.6.4) as

$$\sum_{s=1,2} u_s \frac{\gamma_\mu P_\nu + \gamma_\nu P_\mu}{2} \bar{u}_s = \mathrm{Tr}\left[(\gamma_\alpha p^\alpha + m) \frac{\gamma_\mu P_\nu + \gamma_\nu P_\mu}{2} \right] \tag{6.6.6}$$

$$= \frac{1}{2} \mathrm{Tr}[\gamma_\alpha \gamma_\mu P^\alpha P_\nu + \gamma_\alpha \gamma_\nu P^\alpha P_\mu + m(\gamma_\mu P_\nu + \gamma_\nu P_\mu)], \tag{6.6.7}$$

where we can use the trace properties of the gamma matrices

$$\mathrm{Tr}[\gamma_\rho \gamma_\sigma] = 4\eta_{\rho\sigma} \quad \text{and} \quad \mathrm{Tr}[(\gamma)^n] = 0 \quad \text{for n odd} \tag{6.6.8}$$

and (6.6.4) therefore simplifies to

$$\Gamma^{\mathcal{G}pp}_{\mu\nu} = 4\lambda_{\mathcal{P}} P_\mu P_\nu. \tag{6.6.9}$$

6.6.2 Reggeization of the Propagator

In order to reggeize the propagator one must now also include the higher spin states on the trajectory. In terms of string theory those states correspond to excitations of strings on the curved background. To do so one uses the so-called Virasoro-Shapiro amplitude, which describes scattering of closed strings and is dual to the exchange of the Pomeron trajectory. It also incorporates crossing symmetry (i.e. symmetry under exchanges of s,t and u) and in flat space this amplitude reads for four closed string tachyons

$$\mathcal{A}_c(p_1, p_2, p_3, p_4) = K_c \frac{\Gamma[-a_c(s)]\Gamma[-a_c(t)]\Gamma[-a_c(u)]}{\Gamma[-a_c(t) - a_c(s)]\Gamma[-a_c(t) - a_c(u)]\Gamma[-a_c(u) - a_c(s)]}, \tag{6.6.10}$$

where K_c is a kinematic prefactor, reflecting the scattering of strings with higher spin and $a_c(x)$ is defined as a linear function

$$a_c(x) = a_c(0) + a'_c x. \tag{6.6.11}$$

Writing the u dependence in terms of s and t one has for $2 \to 2$ scattering of particles with equal mass m:

$$\chi \equiv a_c(s) + a_c(t) + a_c(u) = 4a'_c m^2 + 3a_c(0) \tag{6.6.12}$$

and therefore the Virasoro-Shapiro amplitude reads with this redefinition

$$\frac{\Gamma[-a_c(s)]\Gamma[-a_c(t)]\Gamma[a_c(s)+a_c(t)-\chi]}{\Gamma[-a_c(t)-a_c(s)]\Gamma[a_c(t)-\chi]\Gamma[a_c(s)-\chi]}. \tag{6.6.13}$$

Using Stirling's formula for the asymptotics of the gamma functions

$$\Gamma[s+t] = \Gamma[s]s^t \tag{6.6.14}$$

and

$$\lim_{s\to\infty} a(s) = a's \tag{6.6.15}$$

one gets the Regge limit of the Virasoro-Shapiro amplitude

$$e^{-i\pi a_c(t)}\left(a_c's\right)^{2a_c(t)}\frac{\Gamma[-a_c(t)]}{\Gamma[-a_c(t)-\chi]}. \tag{6.6.16}$$

The general propagator which one wants to reggeize here is given by the massive spin-2 propagator

$$\Delta^{\mathcal{G}}_{\alpha\beta,\gamma\delta}(k) = \frac{d_{\alpha\beta,\gamma\delta}(k)}{k^2-m^2_{\mathcal{G}}} \tag{6.6.17}$$

with

$$d_{\alpha\beta,\gamma\delta} = \frac{1}{2}\left(\eta_{\alpha\gamma}\eta_{\beta\delta}+\eta_{\beta\gamma}\eta_{\alpha\delta}-\frac{1}{2}\eta_{\alpha\beta}\eta_{\gamma\delta}\right) \tag{6.6.18}$$

The next step is to compare this stringy result with the traditional parameters of Regge theory, where we have

$$\alpha_c(0)+\alpha_c'm_J^2 = J \tag{6.6.19}$$

and from this one gets for the glueball with $J=2$

$$m^2_{\mathcal{G}} = m_2^2 = -\frac{a_c(0)}{a_c'}, \quad 2a_c(0)+2 = \alpha_{\mathcal{G}}(0) \quad \text{and} \quad 2a_c' = \alpha'_{\mathcal{G}}. \tag{6.6.20}$$

The Regge limit of the Virasoro-Shapiro amplitude is then given by the replacement

$$\frac{1}{t-m_{\mathcal{G}}} \longrightarrow \frac{\alpha'_{\mathcal{G}}}{2}\frac{e^{-i\frac{\pi}{2}\alpha_{\mathcal{G}}(t)}\Gamma[-\chi]\Gamma\left[1-\frac{\alpha_{\mathcal{G}}(t)}{2}\right]}{\Gamma\left[\frac{\alpha_{\mathcal{G}}(t)}{2}-1-\chi\right]}\left(\frac{\alpha'_{\mathcal{G}}s}{2}\right)^{\alpha_{\mathcal{G}}(t)-2}, \tag{6.6.21}$$

with $\alpha_{\mathcal{G}}(t) = 1+\epsilon_{\mathcal{G}}+\alpha'_{\mathcal{G}}t$.

With the values [53]

$$\begin{aligned}\lambda_{\mathcal{P}} &= 8.88\ \text{GeV}^{-1}\\ \alpha'_{\mathcal{G}} &= 0.25\ \text{GeV}^{-2}\\ \epsilon_{\mathcal{G}} &= 0.086\end{aligned} \tag{6.6.22}$$

the propagator for DIS (i.e. $t=0$) is then given by

$$\Delta^{\mathcal{G}}_{\alpha\beta,\gamma\delta}(k) = \frac{1.02\left(-i\alpha'_{\mathcal{G}}s\right)^{\epsilon_{\mathcal{G}}}}{2s}\left(\eta_{\alpha\gamma}\eta_{\beta\delta}+\eta_{\beta\gamma}\eta_{\alpha\delta}-\frac{1}{2}\eta_{\alpha\beta}\eta_{\gamma\delta}\right) \tag{6.6.23}$$

Chapter 7

Results

7.1 Matrix Element and Structure Functions

With the vertices and the propagator defined in the previous sections, we find the hadronic tensor as

$$\begin{aligned}\mathcal{T}^{\mu\nu}(p,q) = i\frac{(-i\alpha'_{\mathcal{G}}W^2)^{\epsilon_{\mathcal{G}}}}{2\pi W^2}\left(-\eta^{\mu\alpha}+\frac{q^\mu q^\alpha}{q^2}\right)\left(-\eta^{\nu\beta}+\frac{q^\nu q^\beta}{q^2}\right)\mathrm{Tr}\big(\mathcal{Q}^2\big)4\lambda_{\mathcal{P}}\Bigg[\frac{t_2^{\mathcal{V}\mathcal{V}}q^4}{M_{KK}^2}(\eta_{\alpha\kappa}\eta_{\beta\lambda}+\eta_{\beta\kappa}\eta_{\alpha\lambda})\\ - t_3^{\mathcal{V}\mathcal{V}}\Big(\eta_{\beta\lambda}q_\kappa q_\alpha+\eta_{\alpha\lambda}q_\kappa q_\beta+\eta_{\alpha\kappa}q_\beta q_\lambda+\eta_{\beta\kappa}q_\alpha q_\lambda-2\eta_{\alpha\beta}q_\kappa q_\lambda-q^2(\eta_{\alpha\kappa}\eta_{\beta\lambda}+\eta_{\beta\kappa}\eta_{\alpha\lambda})\Big)\Bigg]\\ \times\frac{1}{2}\left(\eta^{\kappa\gamma}\eta^{\lambda\delta}+\eta^{\lambda\gamma}\eta^{\kappa\delta}-\frac{1}{2}\eta^{\kappa\lambda}\eta^{\gamma\delta}\right)p_\gamma p_\delta.\end{aligned} \tag{7.1.1}$$

Contracting this expression yields for the t_2-term

$$\frac{q^4}{M_{KK}^2}\left(2p^\mu p^\nu-\frac{1}{2}p^2\eta^{\mu\nu}+p^2\frac{q^\mu q^\nu}{2q^2}-2(p\cdot q)\frac{q^\mu p^\nu+p^\mu q^\nu}{q^2}+2(p\cdot q)^2\frac{q^\mu q^\nu}{q^4}\right) \tag{7.1.2}$$

and for the t_3-term

$$2(p\cdot q)(p^\mu q^\nu+q^\mu p^\nu)-2q^2p^\mu p^\nu-p^2q^\mu q^\nu-(p\cdot q)^2\eta^{\mu\nu}. \tag{7.1.3}$$

We can now plug this result into (4.6.4) and use

$$(-ia)^b+(ia)^b=a^b\Big[(-i)^b+(i)^b\Big]=a^b\Big[e^{ib\frac{\pi}{2}}+e^{-ib\frac{\pi}{2}}\Big]=2a^b\cos b\frac{\pi}{2} \tag{7.1.4}$$

and from this we calculate the hadronic tensor as

$$W^{\mu\nu} = \frac{\lambda_{\mathcal{P}}}{2\pi W^2}\left(\alpha'_{\mathcal{G}}W^2\right)^{\epsilon_{\mathcal{G}}}\cos\left(\frac{\pi}{2}\epsilon_{\mathcal{G}}\right)\mathrm{Tr}\left(\mathcal{Q}^2\right)\Big[\eta^{\mu\nu}\left(4t_3(p\cdot q)^2 - \frac{t_2}{M_{KK}^2}p^2q^4 - 2t_3p^2q^2\right) + q^\mu q^\nu\left(4\frac{t_2}{M_{KK}^2}(p\cdot q)^2 + \frac{t_2}{M_{KK}^2}p^2q^2 + 2t_3p^2\right) - (p^\mu q^\nu + q^\mu p^\nu)4(p\cdot q)\left(\frac{t_2}{M_{KK}^2}q^2 + t_3\right) + p^\mu p^\nu\left(4q^2\right)\left(\frac{t_2}{M_{KK}^2}q^2 + t_3\right)\Big]. \tag{7.1.5}$$

Matching the factors of (4.6.2) we find for the structure functions

$$\begin{aligned} W_1 &= \frac{\lambda_{\mathcal{P}}}{2\pi W^2}\left(\alpha'_{\mathcal{G}}W^2\right)^{\epsilon_{\mathcal{G}}}\cos\left(\frac{\pi}{2}\epsilon_{\mathcal{G}}\right)\mathrm{Tr}\left(\mathcal{Q}^2\right)\left(4t_3(p\cdot q)^2 - 2t_3p^2q^2 - \frac{t_2}{M_{KK}^2}q^4p^2\right) \\ &= \frac{\lambda_{\mathcal{P}}}{2\pi W^2}\left(\alpha'_{\mathcal{G}}W^2\right)^{\epsilon_{\mathcal{G}}}\cos\left(\frac{\pi}{2}\epsilon_{\mathcal{G}}\right)\mathrm{Tr}\left(\mathcal{Q}^2\right)\left(t_3\left(\left(W^2+q^2\right)^2 - 2W^2m_p^2 + m_p^4\right) + \frac{t_2}{M_{KK}^2}q^4m_p^2\right) \end{aligned} \tag{7.1.6}$$

and

$$W_2 = \frac{\lambda_{\mathcal{P}}m_p^2}{2\pi W^2}\left(\alpha'_{\mathcal{G}}W^2\right)^{\epsilon_{\mathcal{G}}}\cos\left(\frac{\pi}{2}\epsilon_{\mathcal{G}}\right)\mathrm{Tr}\left(\mathcal{Q}^2\right)\left(-4q^2\right)\left(\frac{t_2}{M_{KK}^2}q^4 + t_3q^2\right) \tag{7.1.7}$$

and with

$$F_1 = W_1 \quad \text{and} \quad F_2 = -\frac{\nu}{m_p}W_2 = \frac{(p\cdot q)}{m_p^2}W_2$$

we get for the dimensionless structure functions

$$F_1 = \frac{\lambda_{\mathcal{P}}}{2\pi W^2}\left(\alpha'_{\mathcal{G}}W^2\right)^{\epsilon_{\mathcal{G}}}\cos\left(\frac{\pi}{2}\epsilon_{\mathcal{G}}\right)\mathrm{Tr}\left(\mathcal{Q}^2\right)\left(t_3\left(\left(W^2+q^2\right)^2 - 2W^2m_p^2 + m_p^4\right) + \frac{t_2}{M_{KK}^2}q^4m_p^2\right) \tag{7.1.8}$$

and

$$F_2 = \frac{\lambda_{\mathcal{P}}}{2\pi W^2}\left(\alpha'_{\mathcal{G}}W^2\right)^{\epsilon_{\mathcal{G}}}\cos\left(\frac{\pi}{2}\epsilon_{\mathcal{G}}\right)\mathrm{Tr}\left(\mathcal{Q}^2\right)\left(2q^2\right)\left(W^2+q^2-m_p^2\right)\left(\frac{t_2}{M_{KK}^2}q^2 + t_3\right) \tag{7.1.9}$$

7.2 Data

We acquire our data from [54], also see [55] for an in-depth review of the detectors and the definitions of the cross-sections, kinematics and errors. At the Hadron-Elektron-Ring-Anlage (HERA), the deep inelastic scattering of electrons on protons is studied at center-of-mass energies of up to $\sqrt{s} \simeq 320$ GeV. The two collaborations H1 and ZEUS explored

a large phase space in Bjorken x and negative four-momentum-transfer squared Q^2, where the range of these variables for neutral current interactions was:

$$0.045 \leq Q^2 \leq 50000 \text{ GeV}^2 \tag{7.2.1}$$

$$6 \times 10^{-7} \leq x \leq 0.65, \tag{7.2.2}$$

where we are only interested in the region of low x and low $Q^2 \leq 1$ GeV^2. Therefore we are also only considering proton beam energies of $E_p = 920$ GeV and $E_p = 820$ GeV, corresponding to a $\sqrt{s}$ of 318 GeV and 300 GeV, respectively. The electron beam energy, on the other hand, was $E_e \simeq 27.5$ GeV and the beam was longitudinally polarized.

The two detectors H1 and ZEUS both had an almost 4π hermetic coverage, but used different technical solutions and also kinematic reconstructions in order to significantly reduce systematic uncertainties. Both detectors had calorimeters with an inner part to measure electromagnetic energy and identify electrons and an outer part to measure hadronic energy and determine the missing energy. H1 used a liquid-argon calorimeter, whilst ZEUS used a uranium-scintillator. Therefore, H1 was better suited for fine segmentation and was able to identify electrons down to lower energies, whereas the uranium-scintillator made jet studies easier. The backward region of H1 consisted of a lead-scintillating fibre (a.k.a. "spaghetti" calorimeter) and ZEUS used a uranium-scintillator there as well. The field strength of the solenoidal magnetic field used in both detectors was 1.16T and 1.43T and the tracking devices were cylindrical drift chambers in both cases. H1 used two concentric drift chambers, while ZEUS only featured one large chamber. Later on, both detectors also employed a silicon microvertex detector in order to identify electrons in low-Q^2 events.

The DIS cross section depends on $\sqrt{s}$, Q^2 and x, where

$$x = \frac{Q^2}{sy} \tag{7.2.3}$$

and y is the inelasticity of the reaction. For neutral current scattering, the so-called electron method was applied, for which the quantities y and Q^2 were calculated using the variables measured for the scattered electron as

$$y = 1 - \frac{\Sigma_e}{2E_e}, \qquad Q^2 = \frac{P_{T,e}^2}{1-y}, \qquad x = \frac{Q^2}{sy}, \tag{7.2.4}$$

where $\Sigma_e = E'_e(1 - \cos\theta_e)$, E'_e is the energy of the scattered electron, θ_e is the angle with respect to the proton beam and $P_{T,e}$ is its transverse momentum.

Overall, the data consists of 41 data sets, which were then combined into 8 tables, where only the first two cover the region of interest in our low-Q^2 study. This region is covered by data from both experiments, whereas the lowest ($Q^2 \geq 0.045$ GeV^2) only come from ZEUS, where a special tagging device was used. The uncertainties listed in the tables of [54] consist of:

- procedural uncertainties from the choices made in the combination of the results from both experiments.

- experimental uncertainties.
- model and parameterisation uncertainties for the parton distribution functions.

The data provided from HERA contains the variables Q^2, x and σ_{red}.

7.3 Fitting and Calculation of the Couplings

The scripts for calculating the couplings and for fitting the data were coded in `Python` and the following libraries were used:

- `NumPy`
- `lmfit`
- `SciPy`
- `pandas`
- `iminuit`

7.3.1 Couplings

The couplings were calculated using (5.3.13), (6.4.5), (6.4.6),(6.4.7) and (6.3.4). We substitute for the vector meson mode equation

$$Z = \tan(x) \qquad \Longrightarrow \qquad \mathrm{d}Z = \cos^{-2}(x) \tag{7.3.1}$$

and get for (5.3.13)

$$\psi''_{2n}(x) = -M_{2n}\cos^{-\frac{4}{3}}(x)\psi_{2n}(x), \tag{7.3.2}$$

where we introduced the eigenvalue M and are only interested in the even modes of the vector meson fields ψ as they correspond to the non-normalizable modes of the photon. We also get for (6.4.7)

$$\mathcal{J}'' = \cos^{-\frac{4}{3}}(x)\frac{Q^2}{M_{KK}^2}\mathcal{J}. \tag{7.3.3}$$

For the tensor glueball mode equation we use the substitution

$$r = \cos^{-\frac{1}{3}}(x) \qquad \Longrightarrow \qquad dr = \frac{1}{3}\frac{\sin(x)}{\cos^{\frac{4}{3}}(x)}, \tag{7.3.4}$$

which is equivalent, since $1 + Z^2 = \left(\frac{r}{r_k}\right)^6$, cp. (5.3.12), and (6.3.4) then reads

$$T_4''(x) = \cos^{-\frac{4}{3}}(x)\left(\frac{\cos^{\frac{1}{3}}(x)}{\sin(x)}T_4'(x) - \lambda_T T_4(x)\right). \tag{7.3.5}$$

We also introduce the IR boundary at $U = U_{KK}$ as well as the UV boundary at $U = \infty$ for the new coordinates

$$\epsilon = 10^{-8} \tag{7.3.6}$$

$$b_{\mathrm{IR}} = \epsilon \tag{7.3.7}$$

$$b_{\mathrm{UV}} = \frac{\pi}{2} - \epsilon, \tag{7.3.8}$$

where ϵ is the chosen cutoff value.

Since we can solve (7.3.2) and (7.3.5) as initial value problems, we need to introduce the boundary conditions at U_{KK} as

$$\psi_{2n}(b_{\mathrm{IR}}) = 1 \tag{7.3.9}$$
$$\psi'_{2n}(b_{\mathrm{IR}}) = 0 \tag{7.3.10}$$
$$T_4(b_{\mathrm{IR}}) = 1 \tag{7.3.11}$$
$$T'_4(b_{\mathrm{IR}}) = 0. \tag{7.3.12}$$

On the other hand, we solve (7.3.3) as a boundary value problem and set

$$\mathcal{J}'(b_{\mathrm{IR}}) = 0 \tag{7.3.13}$$
$$\mathcal{J}(b_{\mathrm{UV}}) = 1. \tag{7.3.14}$$

In order to find the eigenfunctions we now use `scipy.integrate.solve_ivp` for T_4 and `scipy.integrate.solve_bvp` for $\mathcal{J}$. Since we are not interested in excited glueball states, it is sufficient to only consider the first eigenvalue at $\lambda_T = 2.455$. We now also rewrite (6.4.5) and (6.4.6) as

$$t_2^{\mathcal{V}^*\mathcal{V}^*}(Q_1, Q_2) = \frac{M_{KK}^4}{Q_1^2 Q_2^2} 2\mathcal{N}\kappa \int \mathrm{d}x \, \frac{\left(1+\tan^2(x)\right)^{-\frac{1}{3}}}{\cos^2(x)} \frac{\mathcal{J}'(Q_1, x)}{dZ} \frac{\mathcal{J}'(Q_2, x)}{dZ} T_4(x), \tag{7.3.15}$$

$$t_3^{\mathcal{V}^*\mathcal{V}^*}(Q_1, Q_2) = 2\mathcal{N}\kappa \int \mathrm{d}x \, \frac{\left(1+\tan^2(x)\right)^{-\frac{1}{3}}}{\cos^2(x)} \mathcal{J}(Q_1, x)\mathcal{J}(Q_2, x)T_4(x), \tag{7.3.16}$$

where $\mathcal{N}$ is the factor we obtain from canonical normalization [46][1] and is given by

$$\mathcal{N} = 103.1365217\sqrt{\lambda}N_c M_{KK}. \tag{7.3.17}$$

The factor of 2 stems from the fact that we only integrated the half interval. We then use `scipy.integrate.quad` for numerically integrating those expressions for different values of Q, but with $Q_1 = Q_2$ and store the interpolated result via splines, see figure 7.1.

7.3.2 Fitting

In order to fit the data to the model presented above, first of all we need to translate the given quantities into the quantities used in the model via the relations established in section 4.2, i.e.

$$W^2 = \frac{Q^2}{x} - Q^2 + m_p^2 \tag{7.3.18}$$
$$y = \frac{Q^2}{x\left(s - m_p^2\right)}. \tag{7.3.19}$$

[1] Note that in this paper they defined the numerical value as $\mathcal{N}^{-1}$ rather than $\mathcal{N}$ as given here.

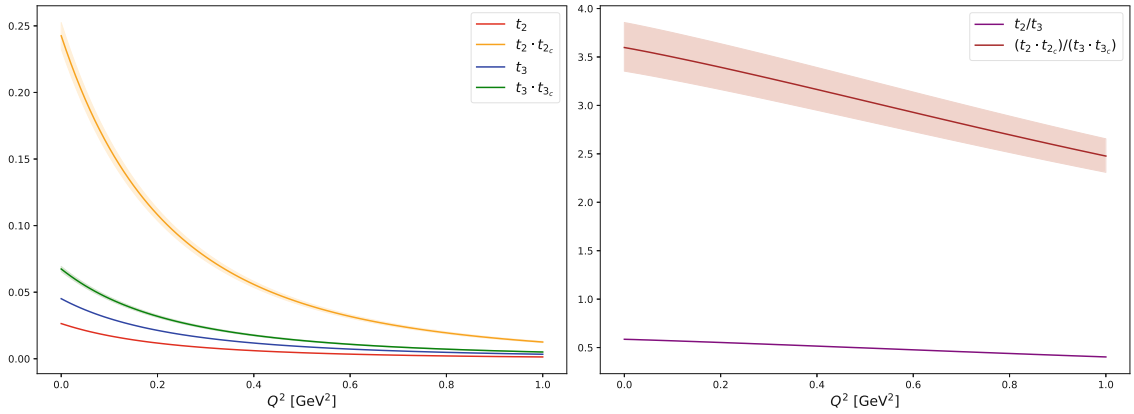

Figure 7.1. (left) The calculated couplings t_2 and t_3 at $M_{KK} = 0.949$ GeV, plotted as functions of Q^2. The scaled versions $t_2 \cdot t_{2_c}$ and $t_3 \cdot t_{3_c}$, obtained from the fit, are also displayed along with the associated error bands, representing the uncertainty in the fitted parameters. (right) The ratio of the two couplings, t_2/t_3, is shown, as well as the scaled ratio $(t_2 \cdot t_{2_c})/(t_3 \cdot t_{3_c})$, including the uncertainties.

Since our model is only valid for values of $Q^2 \to 0$, we are rather restricted in the amount of data points we can use in the fit, as HERA only provided few data points in the region of very small Q^2. The data in the low Q^2 and low x region fitted at HERA show poor χ^2 values, see [54] p. 27f and the best fits of the HERAPDF2.0 analysis were achieved for 15 GeV$^2 \leq Q^2 \leq 150$ GeV^2. Therefore we need to compromise between few data points at low Q^2 and many data points further away from the actual region of interest. In order to do so we compared at different Q^2-cutoff value of the results with respect to their reduced χ^2 values and found the best fit for $Q^2 \leq 0.5$ GeV^2, resulting in $\chi^2_{red} = 0.909$. As is suggested by the plots, deviations to our model predominantly arise for higher values of Q^2, but on the other hand the fitting results turn out to be worse when only considering smaller values of Q^2, as there are too few data points to be included in the fit. The results of the corrections to the parameters t_2 and t_3 can be found in (7.3.20). The plots of the fit for the different $\sqrt{s}$ values are presented in figure 7.2 and 7.3.

The values we get for the correction parameters are further off as initially expected. Whilst t_3 seems to behave rather nicely, the corrective factor for t_2 is off by almost one order of magnitude. Albeit being discouraging for the validity of the model, there are at least some ways of making this result plausible. When one reduces the limit on Q^2 and compares the fit as $Q^2 \to 0$ we notice that the corrective parameter for t_2 also diminishes. But as already mentioned before, the goodness-of-fit analysis shows that the fits also get worse in this region. We therefore conclude that especially t_2 is not easily checked with the model and data presented above, since the fits are always skewed in direction of higher Q^2, instead of lower Q^2, where we assume the model to be valid. In this sense the model and the fitting procedure is not suitable to describe the given data points. Whether this fact can be improved by new and plenty data at $Q^2 \to 0$ is yet to be determined.

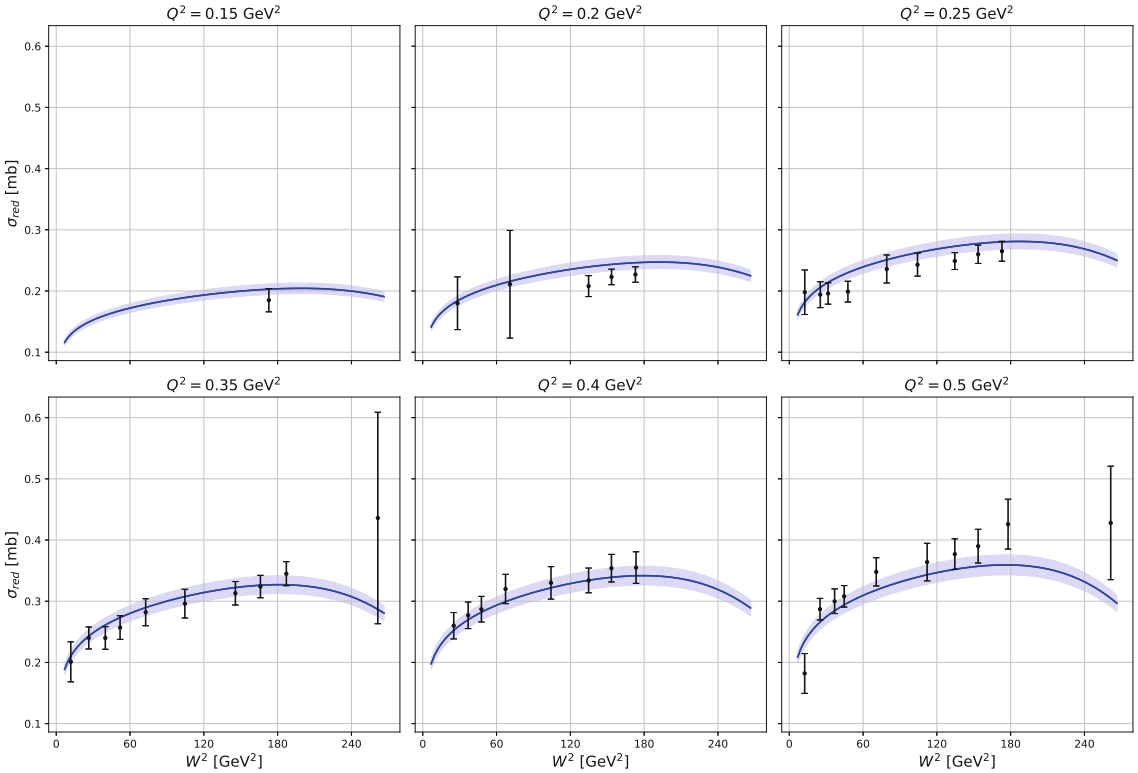

Figure 7.2. Fit for $\sqrt{s} = 318$ GeV. The bands show the error of the parameters as determined by the fit.

The values for the correction parameters and their errors are

$$\begin{aligned} t_{2_c} &= 9.18180 \pm 0.378 \\ t_{3_c} &= 1.49477 \pm 0.043 \end{aligned} \tag{7.3.20}$$

and for the fit we get for 68 datapoints

$$\chi^2 = 61.81745 \tag{7.3.21}$$

$$\chi^2_{red} = 0.90908 \tag{7.3.22}$$

Overall, the fits are in good correspondence with the data. Especially for the parameter t_{2_c}, though, the discrepancy between the calculated value and the needed correction is vast, as can be seen in figure 7.1. From this fact it can be concluded that our calculations yields a sensible form factor behavior, but both couplings fall of too quickly in the WSS model and apparently this effect is more prominent for t_2 as compared to t_3.

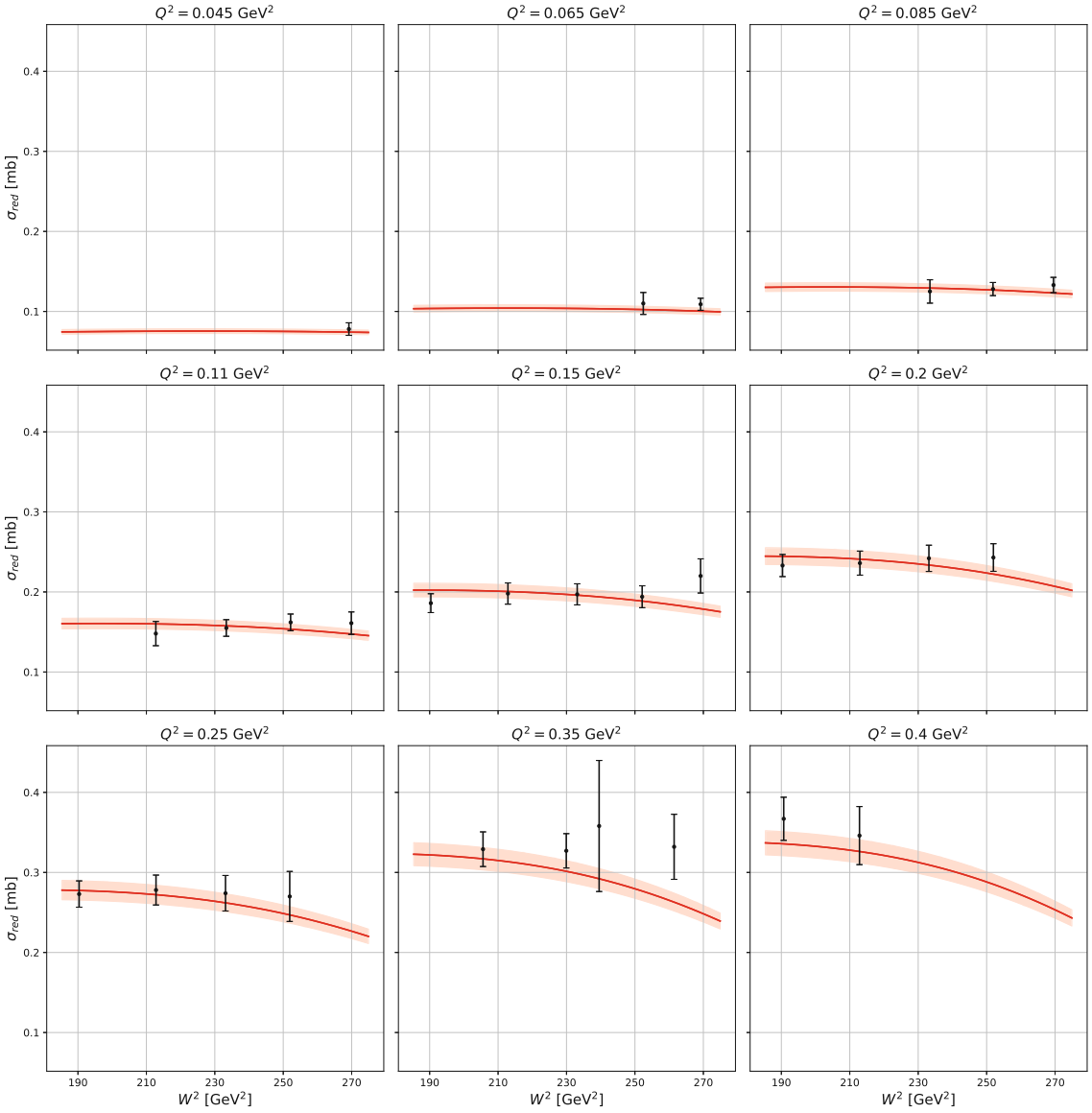

Figure 7.3. Fit for $\sqrt{s} = 300$ GeV. The bands show the error of the parameters as determined by the fit.

7.3.3 Summary

From our study, we conclude that the available data in the region of interest is insufficient to yield meaningful results, particularly in the region where $Q^2 \to 0$, which is the primary focus of our model but remains very sparse in data. The falloff of the couplings in the WSS model is known to be too rapid, and as of the time this study was conducted, there is no clear method to address this issue. To make more sense of the analysis presented above, it is imperative to obtain more data points that can be used for fitting; new experiments capable of probing the required range of virtualities are discussed in the next section. On the other hand, the behavior of the quantities themselves, as calculated in section 7.1,

shows good correspondence with the existing data.

7.4 Future experiments

In this section we will give reference to experiments suitable for further examining the region of low Q^2, see [33, 56, 57].

7.4.1 EIC

The Electron Ion Collider (EIC) is an upcomming accelerator facility situated at Brookhaven National Laboratory on Long Island, New York, and is currently under construction. It will facilitate the most powerful electron microscope in terms of resolving power, intensity and versatility in order to study the structure of atomic nuclei, protons and neutrons. The EIC will be capable of colliding high-energy electron beams with high-energy proton beams or beams of light ions and it features:

- Highly polarized ($\sim 70\%$) electron and proton beams
- Ion beams from deuterons to heavy nuclei (e.g. Au, Pb, U)
- Variable $e+p$ center-of-mass energies $\sqrt{s}$ from 20-140 GeV
- High collision electron-nucleon luminosity of $10^{33} - 10^{34}\text{cm}^{-2}\text{s}^{-1}$
- More than one interaction region

In addition to neutral-current inclusive DIS processes, such as $e + p/A \to e' + X$, the EIC will enable measurements in various other scattering processes. These include charged-current inclusive DIS ($e + p/A \to \nu + X$) at high Q^2, where the electron-quark interaction is mediated by the exchange of a $W^{\pm}$ boson rather than a virtual photon. Another type of process is semi-inclusive DIS ($e + p/A \to e' + h + X$), in which at least one hadron is detected alongside the scattered electron. Furthermore, the EIC will facilitate exclusive DIS ($e + p/A \to e' + \dots$), where all particles involved in the process are measured with high precision. Additional key measurements will include DVCS and deeply virtual meson production, both crucial for probing generalized parton distributions (GPDs).

7.4.2 LHeC

The first ideas of realising an ep collider at CERN date back as early as 1984, but only in 2007 it was found to be feasible to also include this type of reaction to the Large Hadron Collider (LHC) operation besides pp-collisions and hence this setup was called the Large Hadron Electron Collider (LHeC). It is estimated that the earliest possible start of operation of this new collider is in 2032, during the LHC Run 5 period. The achievable center-of-mass energy of about $\sqrt{s} \simeq 1.5$ TeV is expected to allow an insightful study of DIS, especially at low-x. Therefore, the LHeC would be able to vastly extend the kinematic range for DIS experiments. And since it is combined with the hadron beams of the LHC, this new setup would also yield the highest resolutions microscope for examining the actual structure and dynamics inside matter. At low-x it is also capable of investigating the parton

interaction dynamics in a regime, where HERA's energy range was too limited. It will also be able to determine α_s very accurately.

The energy of the electron beam is chosen to be $E_e \simeq 50$ GeV, which is almost double of HERA. The range of virtualities important for the study presented here, $Q^2 \to 0$, can be achieved by reducing E_e to about 10 GeV. With the extension of the Q^2 and x range by more than an order of magnitude and an increased luminosity by a factor of about a thousand, as compared to HERA, the LHeC provides an invaluable tool for studying QCD in a domain, where new phenomena are to be expected. It will also be able to examine the validity of the BFKL evolution.

The LHeC will provide new insight into the one-dimensional structure of nuclei and the proton, as well as multidimensional aspects of the structure of hadrons. This can be achieved by measuring processes with more exclusive final states like the production of jets, semi-inclusive production of hadrons and exclusive processes like DVCS. High precission DIS colliders like LHeC and also EIC therefore allow for investigating the 3D structure of hadrons in great detail. Compared to the EIC, the LHeC will be capable of achieving even smaller values of x, as well as higher values of Q^2, yielding a wider range of about 2 orders of magnitude in both variables. It should also be noted here, that the upgraded version of the LHC, the Future Circular Collider (FCC), will be able to increase the range by yet again roughly one order of magnitude. Another difference between the two colliders is that the EIC will be able to use polarized beams, as was mentioned before, whilst the LHeC will not. For the study conducted here, it is to be expected that the EIC will offer more insights, as it will be capable of achieving lower values of Q^2 than LHeC.

7.4.3 Other Colliders

There are also other colliders targeting a similar kinematic region. Below, we provide a list of upcoming experiments, which is by no means complete. For more detailed information about these experiments, please refer to the references cited.

- Electron-ion collider in China (EicC) [58]
- Electron-Nucleon Collider (ENC) [59]

Appendices

Appendix A

Kinematics and Scattering

A.1 Mandelstam Variables and $\mathcal{S}$-matrix

The Lorentz-invariant Mandelstam variables for the two-body scattering process are defined in the mostly minus convention[1] via

$$s = (p_1 + p_2)^2 \tag{A.1.1a}$$

$$t = (p_1 - p_3)^2 \tag{A.1.1b}$$

$$u = (p_1 - p_4)^2 \tag{A.1.1c}$$

and they satisfy the relation

$$s + t + u = \sum_{i=1}^{4} m_i^2, \tag{A.1.2}$$

with s and t the square of the total energy and the four-momentum transfer between 1 and 3 in the center-of-mass frame, respectively. Since u is not an independent variable, the scattering amplitude can be expressed as $\mathcal{A}(s,t)$.

[1] in the mostly plus convention, which will be used in the main text, those quantities obtain an additional minus sign, see e.g. [60]

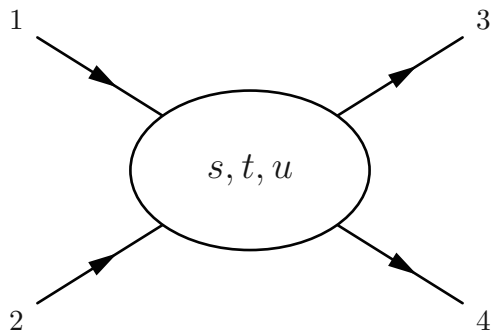

Figure A.1. Scattering of two particles from state $1 + 2$ to state $3 + 4$.

The propability of the transition from initial state $1+2$ or $|i\rangle$ to the final state $3+4$ or $|f\rangle$ is defined such that

$$P_{fi} = |\langle f|\mathcal{S}|i\rangle|^2 = \langle i|\mathcal{S}^\dagger|f\rangle\langle f|\mathcal{S}|i\rangle \tag{A.1.3}$$

With $\sum |f\rangle\langle f|$ being a complete set of orthonormal states. Since the propability of starting with one state and ending up in another state has to be 1 one can write

$$1 = \langle i|\mathcal{S}^\dagger|f\rangle\langle f|\mathcal{S}|i\rangle = \langle i|\mathcal{S}\mathcal{S}^\dagger|i\rangle \tag{A.1.4}$$

and therefore it follows that the $\mathcal{S}$-matrix has to be unitary.

A.2 Optical Theorem

Unitarity of $\mathcal{S}$ is an important feature as it can be used to relate the total cross section and the forward elastic scattering amplitude. The part of the scattering matrix that is not proportional to the identity, thus including all nontrivial interactions, is the transition matrix $\mathcal{T}$ which is defined via

$$\langle f|\mathcal{S}|i\rangle = \langle P_1'P_2'\dots P_n'|\mathcal{S}|P_1P_2\rangle = \delta_{fi} + i(2\pi)^4\delta^4(P^f - P^i)\,\langle f|\mathcal{T}|i\rangle \tag{A.2.1}$$

The orthonormality condition

$$\delta_{ji} = \langle j|\mathcal{S}\mathcal{S}^\dagger|i\rangle = \sum_f \langle j|\mathcal{S}|f\rangle\langle f|\mathcal{S}^\dagger|i\rangle \tag{A.2.2}$$

reads for the $\mathcal{T}$-matrix

$$\langle j|\mathcal{T}|i\rangle - \langle j|\mathcal{T}^\dagger|i\rangle = (2\pi)^4 i\sum_f \delta^4(P^f - P^i)\,\langle j|\mathcal{T}^\dagger|f\rangle\langle f|\mathcal{T}|i\rangle \tag{A.2.3}$$

and for the same initial state as the final state, i.e. $j = i$, we get

$$2\,\mathrm{Im}\,\langle i|T|i\rangle = (2\pi)^4 i\sum_f \delta^4(P^f - P^i)|\langle f|T|i\rangle|^2. \tag{A.2.4}$$

The cross section for the reaction $1+2\to n$ is

$$\sigma_{12\to n} = \frac{1}{4|p_1|\sqrt{s}}\sum (2\pi)^4\, i\sum_f \delta^4(P^f - P^i)|\langle f|T|i\rangle|^2 \tag{A.2.5}$$

Since $\langle i|T|i\rangle$ is the scattering amplitude for the reaction where the direction of motion of the particles is unchanged (in other words $\theta_s = 0$) we get with the assumption of equal masses on the upper and lower halfs of the diagram the variable t to be zero. The relationship between the elastic scattering amplitude $\mathcal{A}(s,t)$ and the total cross section is called the optical theorem and can be expressed as

$$\sigma_{12}^{tot} = \frac{1}{2|p_1|\sqrt{s}}\,\mathrm{Im}\,\mathcal{A}\,(s,t=0)\,, \tag{A.2.6}$$

where the total cross section is defined via

$$\sigma^{tot} = \int \frac{\mathrm{d}\sigma}{\mathrm{d}\Omega}\mathrm{d}\Omega \tag{A.2.7}$$

and can be described as the ratio of the number of interactions per unit time per target particle and the incident flux, see for example [35].

Appendix B

Supergravity

This section will briefly present some concepts of M-theory and Type IIA supergravity, where the latter is proposed as the low-energy limit of the former. Through dualities and compactifications, supergravity is related to string theory and acts as a classical limit in 11 dimensions. The discussion will not delve too deeply into the theory as a whole, but rather aims to explain important concepts used, for example in establishing some concepts used in the Sakai-Sugimoto model of section 5. For further details refer to [61–65]. The calculations for the actual glueball modes, etc., are rather involved and beyond the scope of this discussion. The reader is referred to the papers by, for example, Rebhan et al. and references therein for these calculations in the Sakai-Sugimoto model [41, 43, 46, 51, 66, 67].

B.1 Kaluza-Klein Compactification

The concept of extra dimensions, which are imperceptible to us due to their minuteness, dates back as early as 1914, well before the first considerations of String Theory. The first attempt was a gravitational theory in five dimensions unifying gravity and electromagnetism. This extra dimension, x_4, was compactified on a torus of radius R with

$$x^4 = x^4 + 2\pi R, \tag{B.1.1}$$

resulting in a metric that seperates into $G_{\mu\nu}$, $G_{\mu 4}$ and G_{44}, which correspond to a tensor (the metric), a vector and a scalar field, respectively. In the general case of $D = d+1$, the metric is parameterized as

$$\mathrm{d}s^2 = G^D_{MN}\,\mathrm{d}x^M\,\mathrm{d}x^N = G_{\mu\nu}\,\mathrm{d}x^\mu\,\mathrm{d}x^\nu + G_{dd}\Big(\mathrm{d}x^d + A_\mu\,\mathrm{d}x^\mu\Big)^2, \tag{B.1.2}$$

where μ, ν run over all the noncompact dimensions $0, ..., d-1$. In d-dimensional actions the indices are raised and lowered via $G_{\mu\nu}$ rather than $G^D_{\mu\nu}$. Since the metric (B.1.2) is invariant under translations of x^d, it allows reparameterizations

$$x'^d = x^d + \lambda(x^\mu) \tag{B.1.3}$$

$$A'_\mu = A_\mu - \partial_\mu\lambda \tag{B.1.4}$$

and therefore gauge transformations arise as part of the higher-dimensional coordinate group, which is known as the *Kaluza-Klein* mechanism. In the case of a massless scalar Φ in D-dimensions, the x^d-dependence can be expanded into a complete set,

$$\Phi\big(x^M\big) = \sum_{-\infty}^{\infty} \Phi_n(x^\mu) \exp\left(\frac{inx^d}{R}\right), \tag{B.1.5}$$

with $G_{dd} = 1$ and where the momentum in the periodic dimension is quantized to $p_d = \frac{n}{R}$. Thus the D-dimensional wave equation $\partial_M \partial^M \Phi = 0$ becomes

$$\partial_\mu \partial^\mu \Phi_n(x^\mu) = \frac{n^2}{R^2} \Phi_n(x^\mu) \tag{B.1.6}$$

and the modes Φ_n become an infinite tower of d-dimensional fields of mass

$$-p^\mu p_\mu = \frac{n^2}{R^2}, \tag{B.1.7}$$

which is non-zero for all fields where $p^d \neq 0$. This so-called *Kaluza-Klein* tower of states can only be seen for energies above $\frac{1}{R}$, otherwise only the x^d-independent fields survive and one retains d-dimensional physics. The compact momentum p_d acts as the charge corresponding to the gauge invariance (B.1.4), relating momentum conservation in the fifth dimension with conservation of electric charge. In this example, all the *Kaluza-Klein* states are massive, but in general and, for example, in curved backgrounds, those fields can also be massless while still carrying a Kaluza-Klein charge. The metric component in the compact direction can be redefined as

$$G_{dd} = e^{2\sigma} \tag{B.1.8}$$

and is also called the dilaton. Geometrically speaking, it defines the volume of the compactified dimension. Typically, one works with constant dilatons. In this sense, the dilaton itself is a remnant of compactification and therefore M-theory has none in its spectrum.

B.2 Supergravity to Type IIA Superstring

The expression *supergravity* is shorthand for supersymmetric gravity, which is a field theory combining two very important symmetries, i.e. Poincaré and spacetime supersymmetry invariance. Poincaré invariance combines the properties of the Lorentz group with invariance with respect to translations. SUSY extends the concept of conserved quantities, which are typically scalars, vectors or tensors representing, for example, charge, momentum or stress-energy, by introducing conserved quantities that transform as spinors. As the amount of supercharges does not depend on the representation of the spinor, i.e. Weyl or Majorana, a general supersymmetry algebra has $4N$ supercharges in four dimensions and likewise in any other number of dimensions. In the four-dimensional case, one is also limited to 32 supercharges. This limit of $N = 8$ also holds in higher dimensions, but $d = 11$ is the maximum for which SUSY is possible, since beyond that, the representations become too

large and would allow for unphysical higher-spin particles (spin greater than 2) and multiple gravitons. The bosonic part of the unique supersymmetric action in eleven dimensions reads

$$\mathcal{S}_{11}^{Sugra} = \frac{1}{2\kappa_{11}^2}\int \mathrm{d}^{11}x\,\sqrt{-g}\left(R - \frac{1}{2}|F_4|^2\right) - \frac{1}{12\kappa_{11}^2}\int A_3 \wedge F_4 \wedge F_4, \tag{B.2.1}$$

with the field strength F_4 with its 3-form potential A_3 and the 11-dimensional gravitational constant, defined via

$$2\kappa_{11}^2 = \frac{1}{2\pi}(2\pi\ell_p)^9, \tag{B.2.2}$$

where ℓ_p is the 11-dimensional Planck length. The action for a p-form field is proportional to

$$\int \mathrm{d}^d x\,\sqrt{-g}|F_p|^2 = \int \mathrm{d}^d x\,\frac{\sqrt{-g}}{p!}G^{M_1N_1}\dots G^{M_pN_p}F_{M_1\dots M_p}F_{N_1\dots N_p}. \tag{B.2.3}$$

Compactifying this theory in $d = 11$ on a torus to $d = 10$, as in section B.1, and keeping only the massless fields, one is left with a KK-scalar from $g_{11,11}$, a vector from $g_{\mu 11}$, a 2-form potential from $A_{\mu\nu 11}$ and 3-form potential from $A_{\mu\nu\sigma}$. This is exactly the massless content of the IIA superstring, where the scalar is interpreted as the dilaton. Similar to section B.1, one writes the metric as

$$\begin{aligned} \mathrm{d}s^2 &= G^{11}_{MN}(x^\mu)\,\mathrm{d}x^M\,\mathrm{d}x^N \\ &= G^{10}_{\mu\nu}(x^\mu)\,\mathrm{d}x^\mu\,\mathrm{d}x^\nu + \exp(2\sigma(x^\mu))\left[\mathrm{d}x^{10} + A_\nu(x^\mu)\,\mathrm{d}x^\nu\right]^2, \end{aligned} \tag{B.2.4}$$

Following the procedure presented in section B.1, the action in type IIA string theory therefore reads, after dropping the Chern-Simons term and introducing the kinematics of the dilaton field, as

$$\mathcal{S}_{10}^{\mathrm{IIA}} = \frac{1}{2\kappa_{10}^2}\int \mathrm{d}^{10}x\,\sqrt{-g}e^{-2\Phi}\left(R - \frac{1}{2}e^{2\Phi}|F_4|^2 + 4\partial_M\Phi\partial^M\Phi\right), \tag{B.2.5}$$

where κ_{10}^2 is defined as $\frac{\kappa_{11}}{2\pi R}$, where R is the radius of the compactified dimension.

Bibliography

[1] J.R. Forshaw and D.A. Ross, *Quantum Chromodynamics and the Pomeron*, vol. 9, Oxford University Press (1998), 10.1017/9781009290111.

[2] P.D.B. Collins, *An Introduction to Regge Theory and High Energy Physics*, Cambridge Monographs on Mathematical Physics, Cambridge University Press (7, 2023), 10.1017/9781009403269.

[3] O. Nachtmann, *Elementary Particle Physics: Concepts and Phenomena* (1990).

[4] O. Nachtmann, *Pomeron physics and QCD*, in *Ringberg Workshop on New Trends in HERA Physics 2003*, 2004 [hep-ph/0312279].

[5] V. Barone and E. Predazzi, *High-Energy Particle Diffraction*, vol. v.565 of *Texts and Monographs in Physics*, Springer-Verlag, Berlin Heidelberg (2002).

[6] O. Nachtmann, *Elementary Particle Physics*, Springer Berlin Heidelberg, Berlin, Heidelberg (1990), 10.1007/978-3-642-61281-7.

[7] H. Yukawa, *On the interaction of elementary particles. i*, *Proceedings of the Physico-Mathematical Society of Japan. 3rd Series* **17** (1935) 48.

[8] T. Regge, *Introduction to complex orbital momenta*, *Nuovo Cim.* **14** (1959) 951.

[9] A. Donnachie and P.V. Landshoff, *Elastic Scattering and Diffraction Dissociation*, *Nucl. Phys. B* **244** (1984) 322.

[10] A. Donnachie and P.V. Landshoff, *Dynamics of Elastic Scattering*, *Nucl. Phys. B* **267** (1986) 690.

[11] P.V. Landshoff and J.C. Polkinghorne, *The dual quark-parton model and high energy hadronic processes*, *Nucl. Phys. B* **32** (1971) 541.

[12] M. Diehl, *The Donnachie-Landshoff pomeron and gauge invariance*, *Eur. Phys. J. C* **6** (1999) 503 [hep-ph/9803296].

[13] A. Donnachie and P.V. Landshoff, *Gluon Condensate and Pomeron Structure*, *Nucl. Phys. B* **311** (1989) 509.

[14] P.V. Landshoff and O. Nachtmann, *Vacuum Structure and Diffraction Scattering*, *Z. Phys. C* **35** (1987) 405.

[15] S.K. Domokos, J.A. Harvey and N. Mann, *Pomeron contribution to pp and $p\bar{p}$ scattering in AdS/QCD*, *Phys. Rev. D* **80** (2009) 126015 [0907.1084].

[16] U. Gursoy and E. Kiritsis, *Exploring improved holographic theories for QCD: Part I*, *JHEP* **02** (2008) 032 [0707.1324].

[17] A. Ballon-Bayona, R. Carcassés Quevedo, M.S. Costa and M. Djurić, *Soft Pomeron in Holographic QCD*, *Phys. Rev. D* **93** (2016) 035005 [1508.00008].

[18] A. Ballon-Bayona, R. Carcassés Quevedo and M.S. Costa, *Unity of pomerons from gauge/string duality*, *JHEP* **08** (2017) 085 [1704.08280].

[19] R.C. Brower, J. Polchinski, M.J. Strassler and C.-I. Tan, *The Pomeron and gauge/string duality*, *JHEP* **12** (2007) 005 [hep-th/0603115].

[20] Y.V. Kovchegov and E. Levin, *Quantum Chromodynamics at High Energy*, Cambridge Monographs on Particle Physics, Nuclear Physics and Cosmology, Cambridge University Press (2023).

[21] A.J. Carvalho Amorim de Sousa, *Holography, QCD and Regge Theory*, Ph.D. thesis, Porto U., 2021.

[22] L.N. Lipatov, *Leading logarithmic approximation in QCD*, *Phys. Atom. Nucl.* **67** (2004) 83.

[23] E. Levin and S. Tapia, *BFKL Pomeron: modeling confinement*, *JHEP* **07** (2013) 183 [1304.8022].

[24] D. Britzger, C. Ewerz, S. Glazov, O. Nachtmann and S. Schmitt, *The Tensor Pomeron and Low-x Deep Inelastic Scattering*, *Phys. Rev. D* **100** (2019) 114007 [1901.08524].

[25] A.V. Manohar, *An Introduction to spin dependent deep inelastic scattering*, in *Lake Louise Winter Institute: Symmetry and Spin in the Standard Model*, 3, 1992 [hep-ph/9204208].

[26] A. Deur, S.J. Brodsky and G.F. De Téramond, *The Spin Structure of the Nucleon*, 1807.05250.

[27] C. Adloff, S. Aid, M. Anderson, V. Andreev, B. Andrieu, V. Arkadov et al., *A measurement of the proton structure function f2(x, q2) at low x and low q2 at hera*, *Nuclear Physics B* **497** (1997) 3.

[28] ZEUS collaboration, *Measurement of the proton structure function F2 and sigma-tot (gamma* p) at low q**2 and very low x at HERA*, *Phys. Lett. B* **407** (1997) 432 [hep-ex/9707025].

[29] A. Donnachie and P.V. Landshoff, *Small x: Two pomerons!*, *Phys. Lett. B* **437** (1998) 408 [hep-ph/9806344].

[30] A. Donnachie and P.V. Landshoff, *New data and the hard Pomeron*, *Phys. Lett. B* **518** (2001) 63 [hep-ph/0105088].

[31] A. Donnachie and P.V. Landshoff, *Does the hard pomeron obey Regge factorization?*, *Phys. Lett. B* **595** (2004) 393 [hep-ph/0402081].

[32] C. Ewerz, M. Maniatis and O. Nachtmann, *A Model for Soft High-Energy Scattering: Tensor Pomeron and Vector Odderon*, *Annals Phys.* **342** (2014) 31 [1309.3478].

[33] R. Abdul Khalek et al., *Science Requirements and Detector Concepts for the Electron-Ion Collider: EIC Yellow Report*, *Nucl. Phys. A* **1026** (2022) 122447 [2103.05419].

[34] M. Kachelriess and M.N. Malmquist, *Using Covariant Polarisation Sums in QCD*, *Eur. Phys. J. Plus* **137** (2022) 89 [2107.07187].

[35] M. Thomson, *Modern Particle Physics*, Cambridge University Press (2013).

[36] L.N. Hand, *Experimental investigation of pion electroproduction*, *Phys. Rev.* **129** (1963) 1834.

[37] T. Sakai and S. Sugimoto, *Low energy hadron physics in holographic QCD*, *Prog. Theor. Phys.* **113** (2005) 843 [hep-th/0412141].

[38] T. Sakai and S. Sugimoto, *More on a holographic dual of QCD*, *Prog. Theor. Phys.* **114** (2005) 1083 [hep-th/0507073].

[39] E. Witten, *Anti-de Sitter space, thermal phase transition, and confinement in gauge theories*, *Adv. Theor. Math. Phys.* **2** (1998) 505 [hep-th/9803131].

[40] M. Kruczenski, D. Mateos, R.C. Myers and D.J. Winters, *Towards a holographic dual of large N(c) QCD*, *JHEP* **05** (2004) 041 [hep-th/0311270].

[41] R.C. Brower, S.D. Mathur and C.-I. Tan, *Glueball spectrum for QCD from AdS supergravity duality*, *Nucl. Phys. B* **587** (2000) 249 [hep-th/0003115].

[42] K. Hashimoto, C.-I. Tan and S. Terashima, *Glueball decay in holographic QCD*, *Phys. Rev. D* **77** (2008) 086001 [0709.2208].

[43] F. Brünner, D. Parganlija and A. Rebhan, *Glueball Decay Rates in the Witten-Sakai-Sugimoto Model*, *Phys. Rev. D* **91** (2015) 106002 [1501.07906].

[44] N.R. Constable and R.C. Myers, *Spin two glueballs, positive energy theorems and the AdS / CFT correspondence*, *JHEP* **10** (1999) 037 [hep-th/9908175].

[45] G.T. Horowitz and R.C. Myers, *The AdS / CFT correspondence and a new positive energy conjecture for general relativity*, *Phys. Rev. D* **59** (1998) 026005 [hep-th/9808079].

[46] F. Hechenberger, J. Leutgeb and A. Rebhan, *Radiative meson and glueball decays in the Witten-Sakai-Sugimoto model*, *Phys. Rev. D* **107** (2023) 114020 [2302.13379].

[47] S.K. Domokos, J.A. Harvey and N. Mann, *Setting the scale of the pp and $p\bar{p}$ total cross sections using AdS/QCD*, *Phys. Rev. D* **82** (2010) 106007 [1008.2963].

[48] H. Hata, T. Sakai, S. Sugimoto and S. Yamato, *Baryons from instantons in holographic QCD*, *Prog. Theor. Phys.* **117** (2007) 1157 [hep-th/0701280].

[49] D.K. Hong, M. Rho, H.-U. Yee and P. Yi, *Dynamics of baryons from string theory and vector dominance*, *JHEP* **09** (2007) 063 [0705.2632].

[50] R.M. Wald, *General Relativity*, Chicago Univ. Pr., Chicago, USA (1984), 10.7208/chicago/9780226870373.001.0001.

[51] A. Rebhan, *The Witten-Sakai-Sugimoto model: A brief review and some recent results*, *EPJ Web Conf.* **95** (2015) 02005 [1410.8858].

[52] D.J. Griffiths, *Introduction to elementary particles*, Wiley, Weinheim (2007).

[53] N. Anderson, S. Domokos and N. Mann, *Central production of η via double Pomeron exchange and double Reggeon exchange in the Sakai-Sugimoto model*, *Phys. Rev. D* **96** (2017) 046002 [1612.07457].

[54] H1, ZEUS collaboration, *Combination of measurements of inclusive deep inelastic $e^{\pm}p$ scattering cross sections and QCD analysis of HERA data*, *Eur. Phys. J. C* **75** (2015) 580 [1506.06042].

[55] H1Collaboration and ZEUS Collaboration, "Combination of Measurements of Inclusive Deep Inelastic $e^{\pm}p$ Scattering Cross Sections and QCD Analysis of HERA Data." HEPData (collection), 2015.

[56] LHeC Study Group collaboration, *A Large Hadron Electron Collider at CERN: Report on the Physics and Design Concepts for Machine and Detector*, *J. Phys. G* **39** (2012) 075001 [1206.2913].

[57] LHeC, FCC-he Study Group collaboration, *The Large Hadron–Electron Collider at the HL-LHC*, *J. Phys. G* **48** (2021) 110501 [2007.14491].

[58] D.P. Anderle et al., *Electron-ion collider in China*, *Front. Phys. (Beijing)* **16** (2021) 64701 [2102.09222].

[59] A. Jankowiak, K. Aulenbacher, A. Lehrach, C. Montag, W. Hillert and T. Weis, *Concept for a polarized electron-nucleon collider utilizing the HESR storage ring at GSI/FAIR*, in *Particle Accelerator Conference (PAC 09)*, p. WE6PFP063, 2010.

[60] M. Srednicki, *Quantum Field Theory*, Cambridge University Press (2007).

[61] J. Polchinski, *String theory. Vol. 1: An introduction to the bosonic string*, Cambridge Monographs on Mathematical Physics, Cambridge University Press (12, 2007), 10.1017/CBO9780511816079.

[62] J. Polchinski, *String theory. Vol. 2: Superstring theory and beyond*, Cambridge Monographs on Mathematical Physics, Cambridge University Press (12, 2007), 10.1017/CBO9780511618123.

[63] K. Becker, M. Becker and J.H. Schwarz, *String Theory and M-Theory: A Modern Introduction*, Cambridge University Press (2006).

[64] D.Z. Freedman and A. Van Proeyen, *Supergravity*, Cambridge Univ. Press, Cambridge, UK (5, 2012), 10.1017/CBO9781139026833.

[65] C. Kiefer, *Quantum Gravity*, in *Springer Handbook of Spacetime*, A. Ashtekar and V. Petkov, eds., pp. 709–722 (2014), DOI.

[66] F. Brünner, J. Leutgeb and A. Rebhan, *A broad pseudovector glueball from holographic QCD*, *Phys. Lett. B* **788** (2019) 431 [1807.10164].

[67] F. Brünner and A. Rebhan, *Holographic QCD predictions for production and decay of pseudoscalar glueballs*, *Phys. Lett. B* **770** (2017) 124 [1610.10034].

Acknowledgments

I would like to start by sincerely thanking Florian Hechenberger for his constant availability and willingness to help throughout this process. Florian, your guidance and readiness to tackle any questions I had, no matter how small, made a significant impact on my progress. Your support and encouragement were deeply appreciated.

A special thanks to my parents for their unwavering support, both financially and emotionally, during this challenging time. Your understanding and belief in me were invaluable, especially during moments of doubt. I'm truly grateful for everything you have done to help me succeed.

I also want to express my gratitude to Lisa, who supported me through the greater part of this journey. Your patience, understanding, and motivation were a constant source of strength. You never put me under pressure and always found ways to encourage me, no matter how tough things got. For that, I will always be thankful.

I would also like to thank my friends Lukas and Martin. You both were always there to listen when I needed to talk through ideas or simply needed to vent. Your support made the tougher moments of this journey more manageable.

Lastly, I want to acknowledge everyone who played a role in this thesis, from my professors and colleagues to fellow students who offered feedback and advice along the way. Your contributions, whether large or small, helped shape this work, and for that, I'm thankful.